E-20-M96

Final Report

Vertical Profiles of the Atmospheric Boundary Layer & Upper Air for the Southern Great Plains 1997 Field Experiment

Christa D. Peters-Lidard, PI
Luke H. Davis

Georgia Institute of Technology
School of Civil and Environmental Engineering
Atlanta, Georgia

Sponsor:

National Aeronautics and Space Administration
Goddard Space Flight Center
Greenbelt, Maryland

Report Date:

October 5, 1999

Period of Performance:

15 July 1997—15 July 1999

ABSTRACT

From June 18 to July 17, 1997 (Day 169 to 198), the Georgia Institute of Technology (Georgia Tech) and NOAA's National Severe Storms Laboratory (NSSL) jointly operated a tethersonde system at the DOE ARM/CART Central Facility as part of the Southern Great Plains 1997 Hydrology Experiment (SGP97). The primary role of the tethersonde system was to acquire high-temporal and vertical resolution profiles of temperature, humidity, pressure, and wind speed and direction in the lower atmospheric boundary layer. The tethersonde data collection consisted of ascent-descent sequences. Ascents were initiated hourly from 0700 local time (CDT) through 1100 CDT. Each ascent/descent sequence lasted approximately 45 minutes, yielding two profiles per hour in the morning hours. In the afternoon, ascents were initiated every one and one-half hours from 1230 CDT to 1700 CDT, winds permitting. Samples were obtained at a rate of one every 10 seconds, which yielded a 2-5 meter vertical resolution in the atmosphere. The rise rate typically varied from 0.2-0.5 m/s. The tethersonde could not be deployed in winds greater than 15 knots. Due to the windy conditions in Oklahoma, the tethersonde could be operated on only 16 days of the experiment. The maximum altitude attained during the experiment was 993 m AGL on July 6, 1997, although typical maximum altitudes for each ascent/descent sequence were significantly less due to wind. This final report documents the tethersonde program, including quality control and quality assurance procedures, as well as applications of the work including regional flux estimation. It will serve as the official documentation of the tethersonde data transferred in September 1998 to the Distributed Active Archive Center at the NASA Goddard Space Flight Center.

TABLE OF CONTENTS

LIST OF TABLES

LIST OF FIGURES

LIST OF VARIABLES

A	Entrainment parameter
A_{Betts}	Betts entrainment parameter
A_{Ecor}	Eddy correlation entrainment parameter
$A_{Tennekes}$	Tennekes entrainment parameter
$_c$	Corrected
C_p	Specific heat of dry air at constant pressure
$_{fa}$	Free atmosphere level
G	Ground heat flux
H	Sensible heat flux
$_i$	Inversion level
L	Monin-Obukhov length
L_v	Latent heat of vaporization
LE	Latent heat flux
q	Specific humidity
RH	Relative humidity
Ri	Gradient Richardson number
Ri_B	Bulk Richardson number
Rn	Net radiation
S_q	Net moisture source term
S_Θ	Net heat source term
$_s$	Surface level
t	Time
T	Dry bulb temperature
T_w	Wet bulb temperature
u	Horizontal advection
u_*	Surface shear velocity
v	Horizontal advection
ν_q	Molecular diffusivity for water vapor in the air
ν_Θ	Thermal diffusivity
w	Vertical advection
$w'q'$	Kinematic moisture flux
$w'\Theta'$	Kinematic heat flux
x	Length
y	Width
z	Height
z_h	Heat roughness length
z_m	Momentum roughness length
z_v	Water vapor roughness length
β	Bowen ratio

$\delta\epsilon$	Virtual temperature conversion parameter
γ	Inversion strength (slope of the potential temperature profile in the free atmosphere)
ρ	Density of moist air
ϕ_h	Nondimensional profile functions of heat
ϕ_m	Nondimensional profile functions of momentum
ϕ_v	Nondimensional profile functions of water vapor
Ψ_h	Heat stability correction function
Ψ_m	Momentum stability correction function
Ψ_v	Water vapor stability correction function
τ_o	Surface shear stress
Θ	Potential temperature

INTRODUCTION

Interactions between the land surface and the atmosphere strongly influence both atmospheric boundary layer (ABL) structure and cloud development. These interactions are strongly controlled by surface soil moisture—a quantity which is difficult to measure over large spatial and temporal scales. To date, our process representations of soil moisture and heat exchange have been tested only against a small number of field experiment data bases which are typically of short duration (1-2 weeks) and/or limited spatial extent (<500 km^2). However, as the era of NASA's Earth Observing System (EOS) approaches, we should be capable of monitoring soil moisture and temperature over time and space scales consistent with medium range weather forecast and general circulation models. Moreover, these datasets will be most useful when they can be incorporated directly into coupled hydrologic-atmospheric models and shown to improve weather forecasts, climate prediction and water resources planning.

The Southern Great Plains 1997 (SGP97) Field Experiment was conducted to provide a remotely sensed soil moisture data set unique in its spatial and temporal extent. Aircraft and surface flux measurements support studies of the relationships of spatial boundary layer structure and spatial variability in soil moisture. The atmospheric sounding program in SGP97, including the Georgia Tech tethersonde program, was designed to provide information on the vertical structure of the atmospheric boundary layer. Applications of this information include the use of boundary layer budget methods and surface layer similarity theory to estimate regional fluxes, atmospheric corrections for thermal remote sensing, and boundary and initial conditions for coupled atmospheric-hydrologic modeling.

detailed surface layer profiles will support applications of surface layer similarity theory (Davis, 1999), and boundary layer profiles will support additional studies of entrainment parameterizations.
Ultimately, the modeling studies made possible by these measurements may lead to an increased understanding of the role of soil moisture in cloud development and improved parameterizations of subgrid processes in atmospheric models.

DATA COLLECTION AND PROCEDURE

Introduction

During the Southern Great Plains 1997 (SGP97) Hydrology Experiment, both tethersonde and radiosondes were launched and recorded atmospheric vertical profiles of heat (temperature) and moisture (humidity), which are used to develop regional

evapotranspiration estimates. Several flux stations were also on site and recorded the surface sensible and latent heat fluxes during the experiment. Included in this section are descriptions of the experiment and on-site instrumentation as well as the quality controls used to validate the data and the existing environmental conditions.

Experiment Description

The SGP97 Hydrology Experiment was conducted from June 18 to July 17, 1997 (Day 169 to 198) over the domain shown in Figure 1, which includes the Department of Energy (DOE) Atmospheric Radiation Measurement Program (ARM) Cloud and Radiation Testbeds (CART), El Reno, and Little Washita regions. This domain is typical of the Southern Great Plains region, contains both the Oklahoma Mesonet and Little Washita Micronet with the ARM/CART facilities, and has undergone several previous experiments with the collected historical data readily available to researchers. Based on some of these earlier experiments, the main purpose of SGP97 is to analyze the role of soil moisture in the local energy budget at the surface and the role of mesoscale variability on the development of the ABL. Along with the DOE ARM/CART staff, participants in the SGP97 included National Aeronautics & Space Administration (NASA), United States Department of Agriculture (USDA), and several researchers from universities.

Table 1: List of DOE ARM/CART boundary facilities and central facility radiosonde and tethersonde launch sites, with elevation, latitude, and longitude

Site Name	Location	Elevation (m MSL)	Latitude (Decimal Degrees)	Longitude (Decimal Degrees)
BF1	Hillsboro, KS	447	38.305 N	97.301 W
BF4	Vici, OK	622	36.071 N	99.204 W
BF5	Morris, OK	217	35.688 N	95.856 W
BF6	Purcell, OK	344	34.969 N	97.415 W
CF1 (Radiosonde)	Lamont, OK	313	36.609 N	97.487 W
CF1 (Tethersonde)	Lamont, OK	313	36.606 N	97.485 W

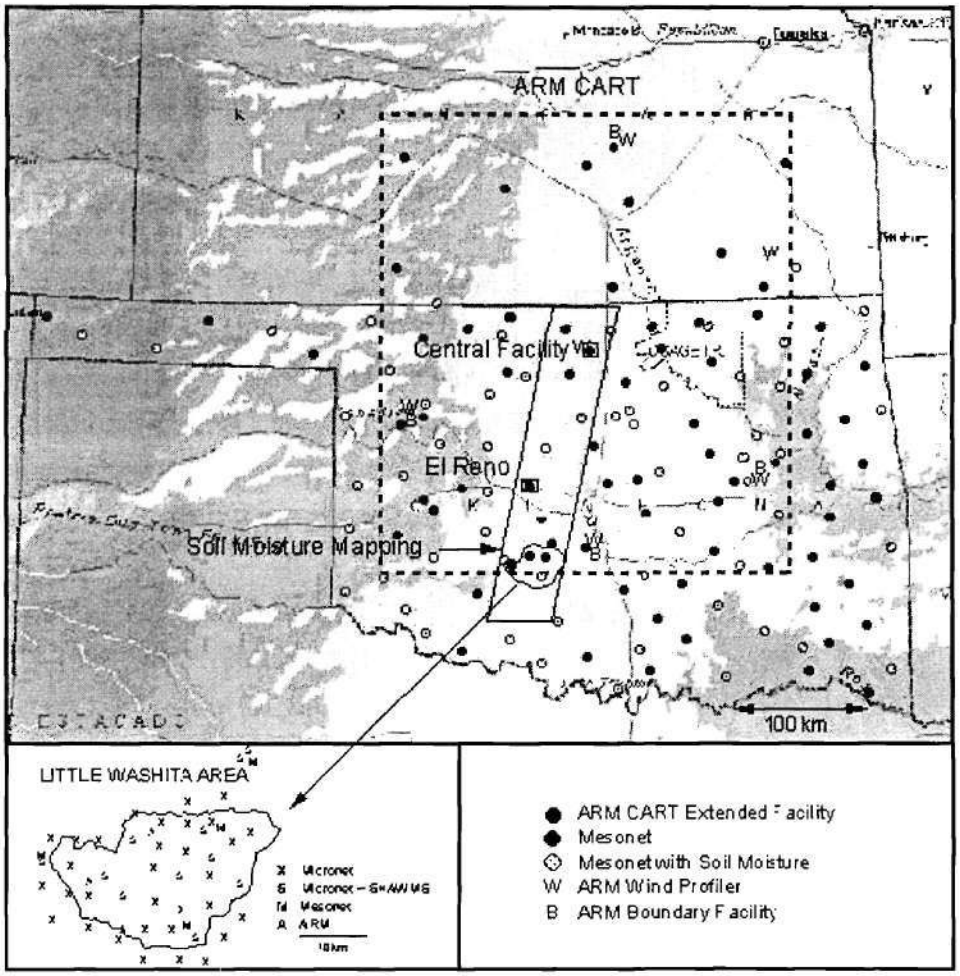

Figure 1: Southern Great Plains 1997, SGP97, Hydrology Experiment domain

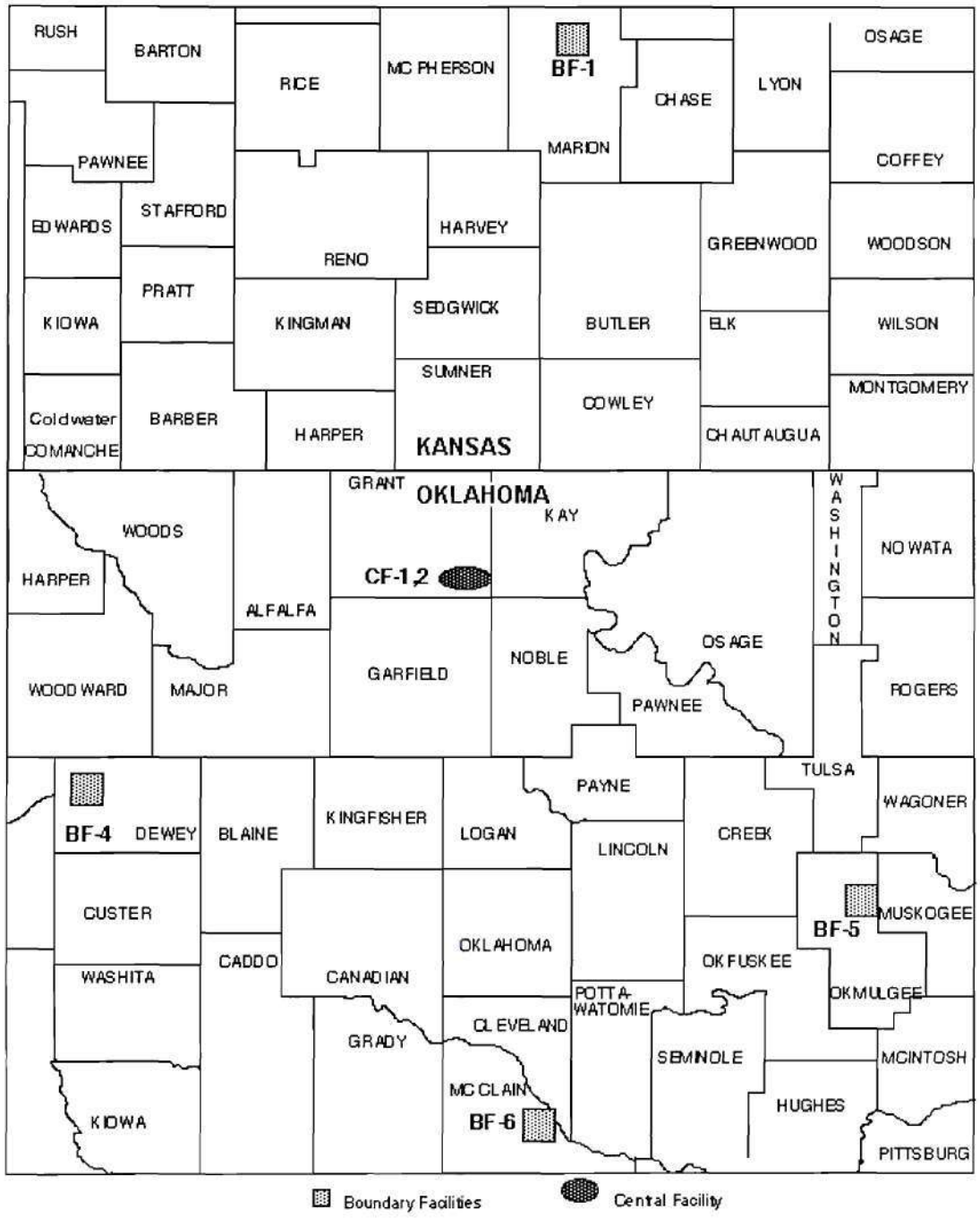

Figure 2: DOE ARM/CART central (CF-1,2) and boundary (BF-1,4,5,6) facilities

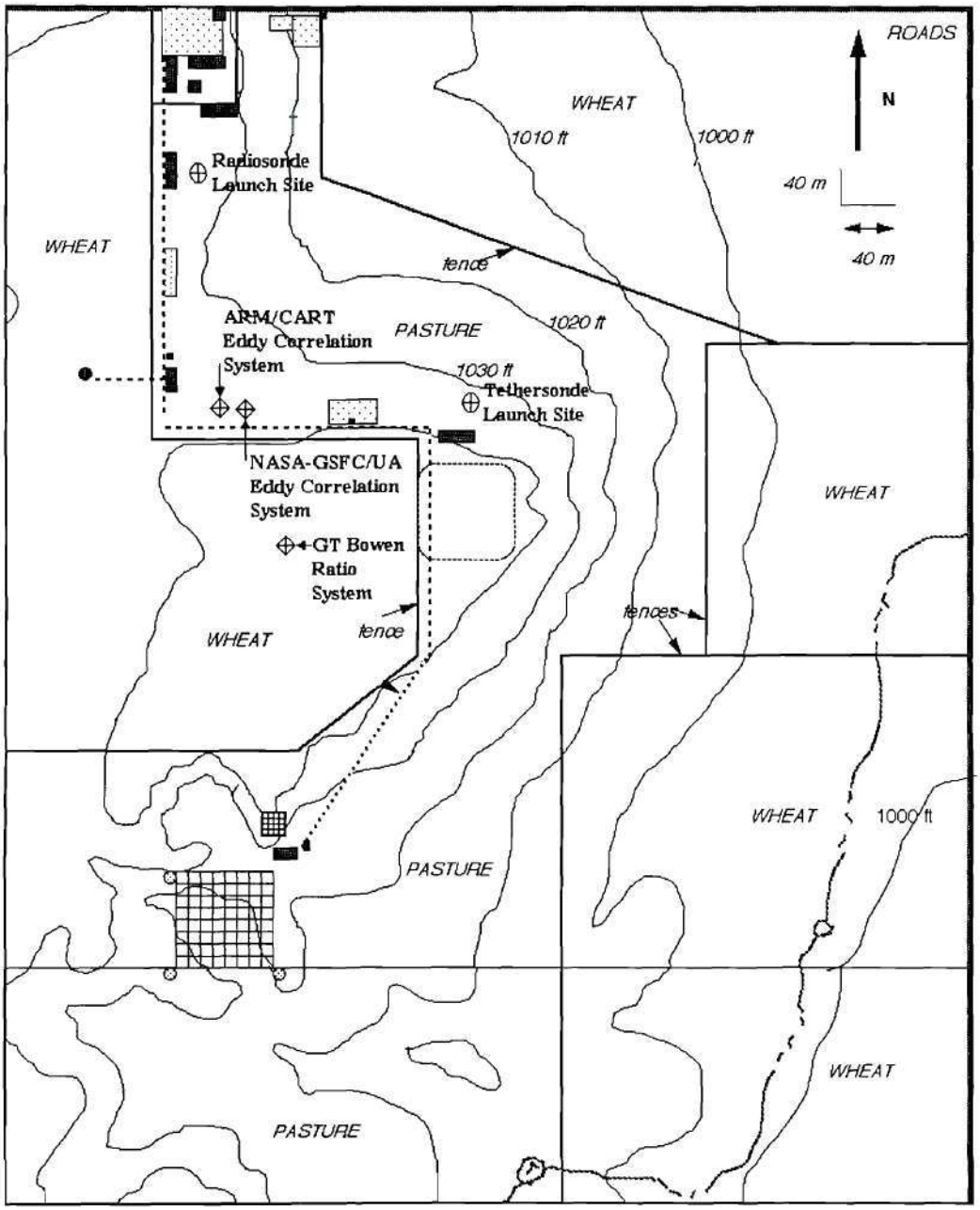

Figure 3: DOE ARM/CART central facility with the radiosonde and tethersonde launch sites, the ARM/CART and NASA-GSFC/UA eddy correlation systems, and the Georgia Tech Bowen ratio system

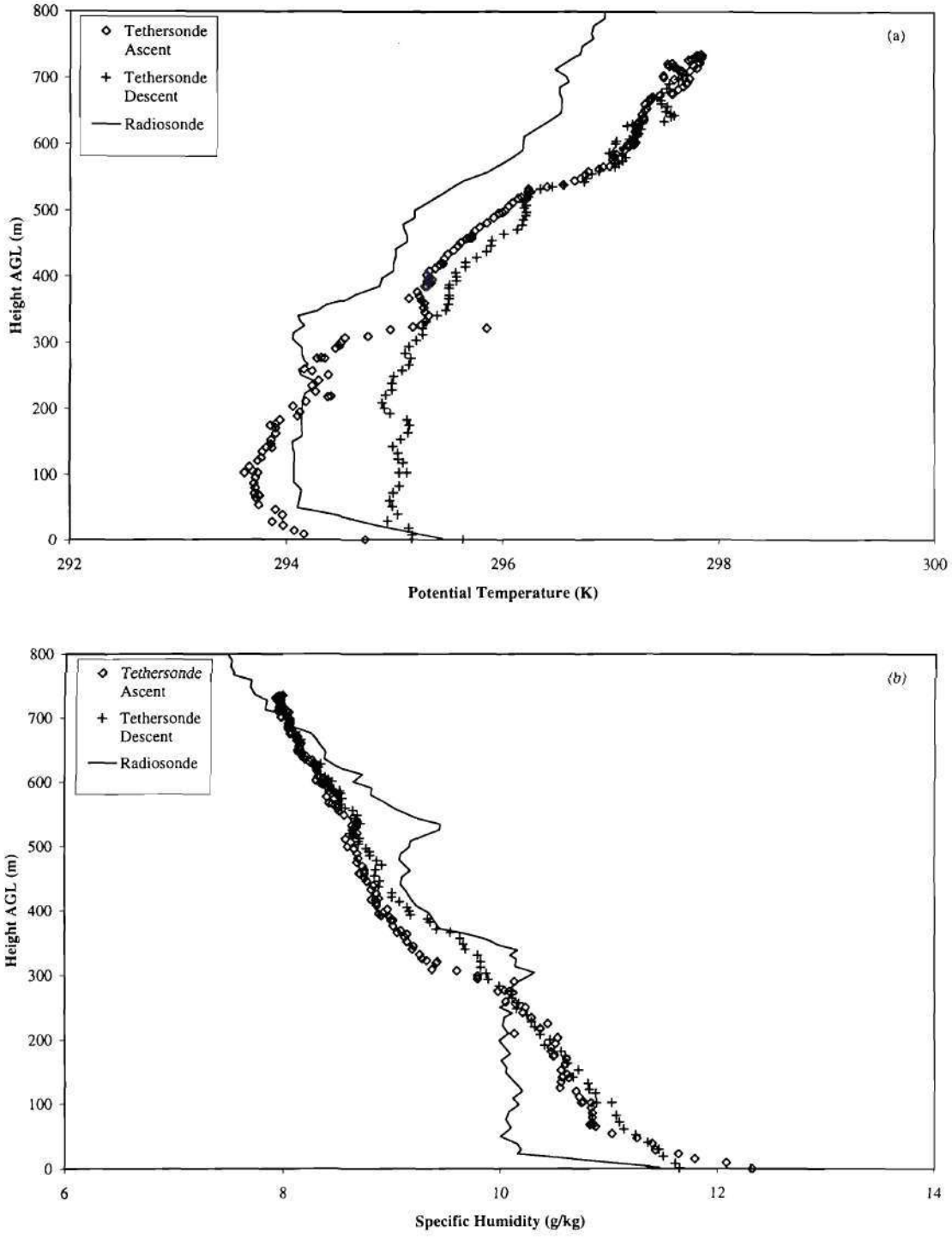

Figure 4 (a) & (b): Potential temperature, Θ, and specific humidity, q, profiles on Day 186 (July 5, 1997) for the tethersonde 1401 GMT ascent and 1430 GMT descent and radiosonde 1429 GMT ascent

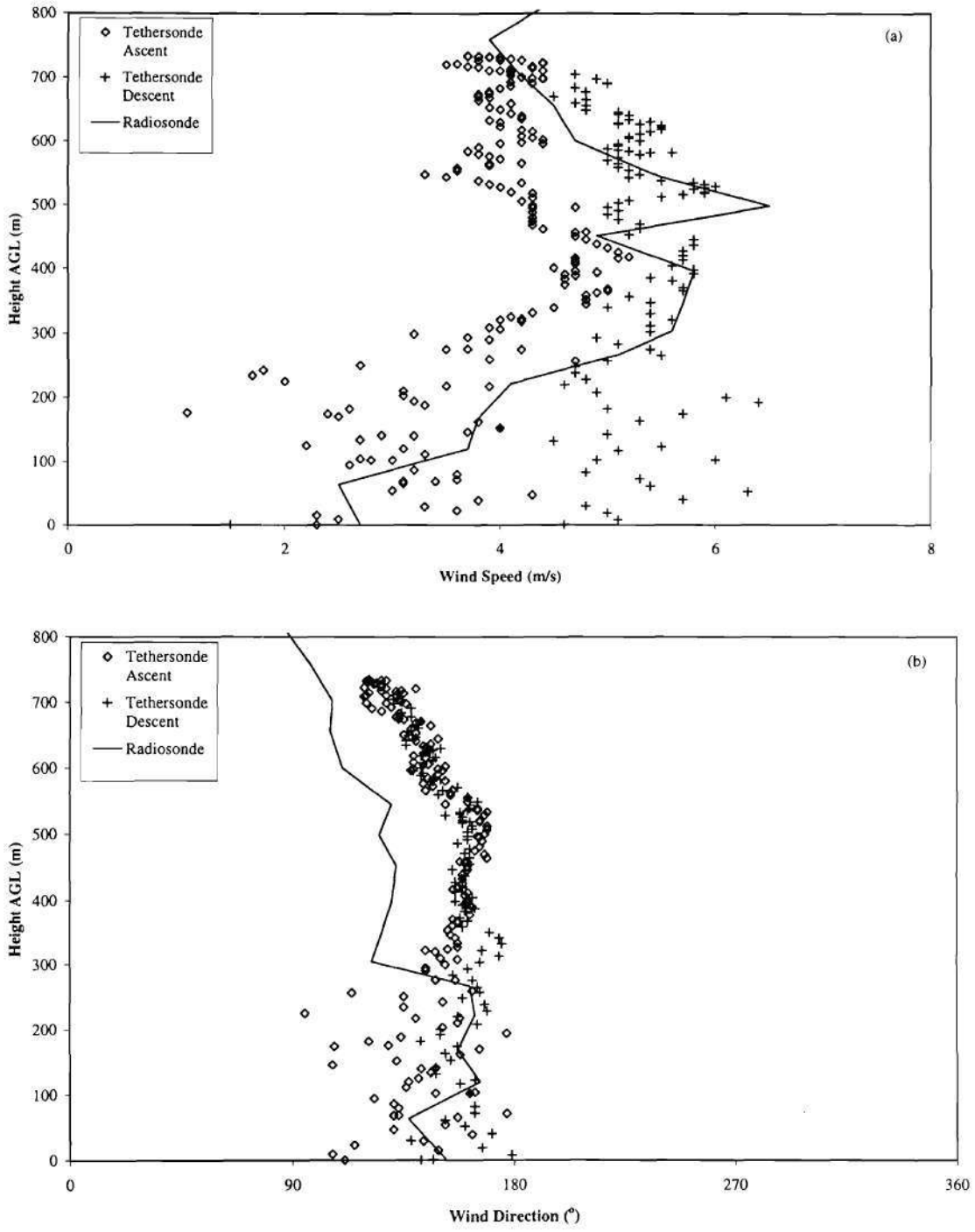

Figure 5 (a) & (b): Wind speed and direction profiles on Day 186 (July 5, 1997) for the tethersonde 1401 GMT ascent and 1430 GMT descent and radiosonde 1429 GMT ascent

As shown in Figure 2, the ARM/CART site consists of a heavily instrumented central facility, 4 boundary facilities, 22 extended facilities (not shown), and 3 intermediate facilities (also not shown) with the locations of the central and boundary facilities summarized in Table 1. Georgia Tech, along with the National Oceanic and Atmospheric Administration's (NOAA's) National Severe Storms Laboratory (NSSL), deployed both a tethersonde and Bowen Ratio system throughout the duration of SGP97 to record atmospheric vertical profiles of heat and moisture and surface flux data, respectively. Figure 3 shows the launch sites of both the tethersonde and radiosondes as well as the eddy correlation systems on site. An example of the tethersonde data, subjected to the quality controls described in a later section, includes the potential temperature and specific humidity profiles in Figures 4 (a) and (b) and wind speed and direction profiles in Figures 5 (a) and (b) along with available ARM/CART radiosonde data for July 5, 1997 (Day 186).

Tethersonde

Georgia Tech and NOAA NSSL jointly operated a tethersonde system when environmental conditions permitted during SGP97. The tethersonde system in Figure 6 is manufactured by Atmospheric Instrumentation Research, Inc.(AIR) and consists of an Atmospheric Data Acquisition System (ADAS) model AIR-3A; two meteorological sensor packages, known as AIRsondes, which are powered by a 9 volt alkaline battery; two helium filled balloons of varying sizes; a 1000-meter tetherline; and a heavy-duty winch. A manual dial on the winch controls the speed of the tethersonde ascent and descent.

The AIRsondes contain dry and wet bulb thermistors to record temperature and solve for humidity using the psychrometric equation, an aneroid capacitance barometer to determine pressure, and a three-cup anemometer with a magnetic compass for wind speed and direction. Both thermodynamic and wind data were recorded at a rate of ten seconds, yielding a 2-5 meter vertical resolution with a typical rise rate between 0.2-0.5 meters per second.

The tethersonde can only be deployed in light winds (less than 10 meters per second) which limited operations to sixteen days of flights during SGP97, as listed in Table 2. Each flight consisted of an ascent-descent sequence with ascents beginning at 0700 local time (CDT) and continued hourly through 1100 CDT in the morning hours to capture the ABL growth. During the afternoon, ascents were initiated every one and one-half hours starting at 1230 CDT and lasting until 1700 CDT.

The tethersonde system did not experience many problems during the experiment with the exception of the 0700 CDT flight on June 25, 1997 (Day 176). The first AIRsonde began quickly losing data during the ascent due to a battery drain within the sensor package. A second AIRsonde replaced this instrument for the remainder of the SGP97 tethersonde flights.

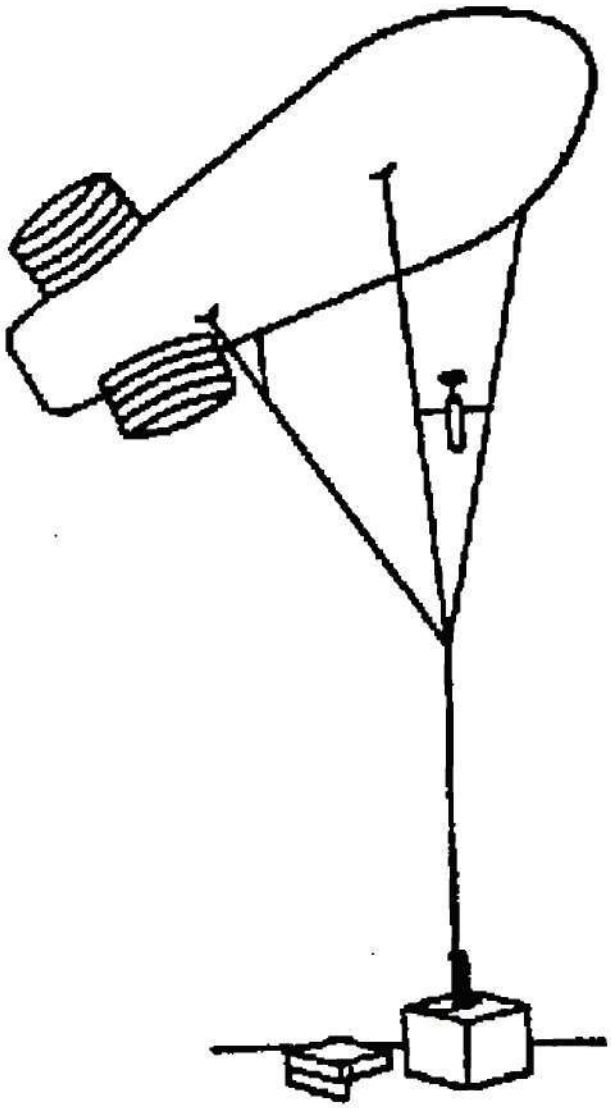

Figure 6: Tethersonde system including balloon, AIRsonde, 1000-meter tetherline, and heavy-duty winch

The tethersonde was launched at least once for each of the sixteen days listed in Table 2. Considering the number of flights per day, maximum altitude achieved, and other factors such as weather conditions, each day of tethersonde flights was assigned one of the following rankings: "Gold", "Silver", "Bronze", or "Other" with the corresponding ranking criteria listed in Table 3. Detailed information for each flight can be found in several tables in Appendix A. Table A.1 contains the inversion height and pressure, and profile average wind speed and direction recorded by the tethersonde. Summary data of the potential temperature and specific humidity at the inversion height, start of free atmosphere, and profile average can be found in Tables A.2 and A.3, respectively.

Radiosondes

ARM/CART released disposable radiosondes, also referred as the Balloon-Borne Sounding System (BBSS), for the duration of SGP97 at the central and boundary facilities listed in Table 1. All of the ARM/CART radiosondes were Vaisala Model RS80-15LH with a disposable balloon. The central facility contained a PC-CORA ground station, while each of the boundary facilities used a Digi-CORA Model MW-11 ground station.

The radiosondes contain a capacitive bead to record temperature, H-HUMICAP thin film capacitor to measure humidity, an aneroid capacitive barometer to determine pressure, and utilize a Loran-C navigation system for the wind speed and direction. Thermodynamic samples were recorded at two second intervals with wind data every ten seconds, yielding a 10-15 meter vertical resolution with a typical rise rate around 5 meters per second.

The radiosonde can be deployed in any wind conditions throughout SGP97. Initiating at 0200 CDT daily, radiosondes were launched from the central facility and all four boundary facilities, continuing every three hours. The central facility radiosonde profiles were compared with temporally corresponding tethersonde profiles and are analyzed in the quality control section of this report.

Flux Stations

There were several surface flux stations set up at the ARM/CART central facility during a portion or all of SGP97. Both the NASA-Goddard Space Flight Center (GSFC) with the University of Arizona (UA) and ARM/CART maintained eddy correlation systems on site near the northern edge of a wheat field that measured each term of the energy budget independently and averaged them over thirty minute time intervals. The University of Wisconsin-Madison (UWM) had a roving (mobile) eddy correlation system that was used to calibrate all of the other instruments through a brief collocation period during SGP97 subject to the constraint that the energy budget was closed in post processing. Georgia Tech also maintained a Bowen ratio system at the central facility for the duration of SGP97. All of the aforementioned flux data is available to the public on the NASA-GSFC Distributed Active Archive Center (DAAC) site (http://daac.gsfc.nasa.gov/CAMPAIGN_DOCS/SGP97/sgp97.html).

Table 2: Tethersonde flights during SGP97 with maximum altitude and corresponding pressure achieved that day as well as assigned ranking

Date	DOY	Number of Flights	Maximum Altitude (m AGL)	Pressure at Maximum Altitude (mb)	Ranking
6/18/97	169	5	600	908.8	Silver
6/19/97	170	2	121	959.3	Other
6/22/97	173	3	619	909.3	Bronze
6/25/97	176	7	738	895.4	Gold
6/26/97	177	2	486	925.7	Other
6/27/97	178	7	700	901.3	Silver
6/28/97	179	1	212	948.4	Other
6/29/97	180	1	200	950.2	Other
7/2/97	183	2	658	901.0	Other
7/3/97	184	8	566	910.5	Silver
7/4/97	185	5	675	904.4	Bronze
7/5/97	186	9	778	893.4	Gold
7/6/97	187	8	993	869.6	Gold
7/14/97	195	6	790	890.6	Gold
7/15/97	196	1	330	940.7	Other
7/16/97	197	8	697	900.6	Gold

Table 3: Tethersonde flight rankings and corresponding criteria

Rank	Criteria
Gold	>7 flights/day Calm to light winds Altitude > 700 m AGL
Silver	5-6 flights/day Light to moderate winds Altitude 500-700 m AGL
Bronze	3-4 flights/day Moderate to high winds Altitude < 500 m AGL
Other	< 3 flights/day High winds Miscellaneous problems/weather conditions

Eddy Correlation

The NASA-GSFC/UA eddy correlation system was deployed at the central facility from July 2 to July 17, 1997 (Day 183 to 198). This eddy correlation system consisted of a Radiation and Energy Balance Systems (REBS) Q97301 net radiometer, 3-D Solent sonic anemometer 1012R2A, Li-Cor LI-6262 CO2/H2O analyzer, REBS HFT3-L soil heat flux transducers, and Campbell Scientific 2X2 (TCAV-L35) averaging thermocouples.

An ARM/CART eddy correlation system is maintained at the central facility and recorded flux data throughout the entire experiment. The system consists of a REBS Q*7.1 net radiometer, 3-D sonic anemometer, Applied Technologies Inc. Model SWS-211/3Sx Analytic Applications Inc. Model M100 infrared hygrometer, MINCO Products, Inc., platinum resistance temperature detector, and REBS Model #STP-1, MINCO Model # XS11PA40T260X36(D) with soil heat flow probes.

UWM used a "roving" eddy correlation system for comparison with the other flux stations, including both eddy correlation and Bowen ratio systems, and was on-site from July 3 to July 6, 1997 (Day 184 to 187). The UWM system consisted of a Kipp & Zonen CNR1 net radiometer to verify the net radiation values recorded by the other flux stations and a Campbell Scientific 3-D sonic anemometer (CSAT3) with krypton hygrometer (KH20).

The NASA-GSFC/UA and ARM/CART eddy correlation systems are utilized as a network to represent the regional surface values of both sensible and latent heat. In order to validate each instruments dataset, the UWM linearly calibrated net radiation with all of the flux stations and found a site-average ground heat flux to provide the same available energy for each thirty minute temporal measurement. According to the UWM analysis, the NASA-GSFC/UA system measured questionable latent heat flux values leading to inaccurate Bowen ratios. Therefore the modified available energy and measured heat flux allowed for a modified latent heat flux solved as a residual. For the ARM/CART dataset, the original measured Bowen ratio was assumed to be correct and used to solve for modified sensible and latent heat fluxes. The average diurnal cycle of sensible (H) and latent heat (LE) fluxes from July 2 to July 17, 1997 (Day 183 to 198) for SGP97 are displayed in Figure 7 (a) and (b). The NASA-GSFC/UA eddy correlation system typically measured lower sensible heat fluxes and higher latent heat fluxes than the ARM/CART eddy correlation system. Both the sensible and latent heat root mean square error between the two instruments equals $\pm$ 62 W/m^2.

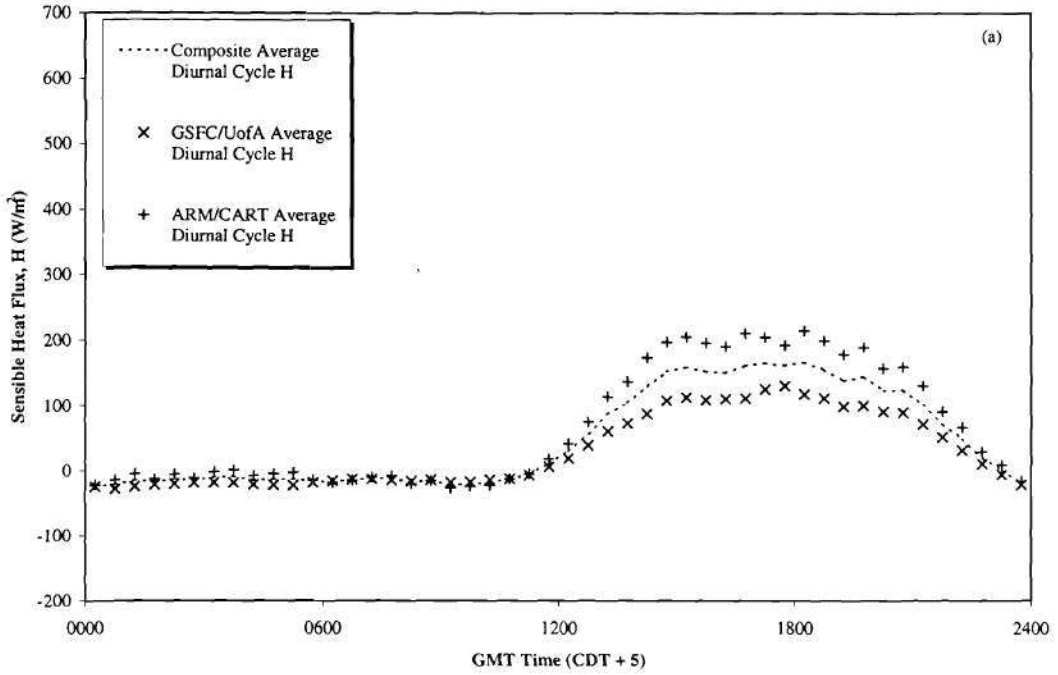

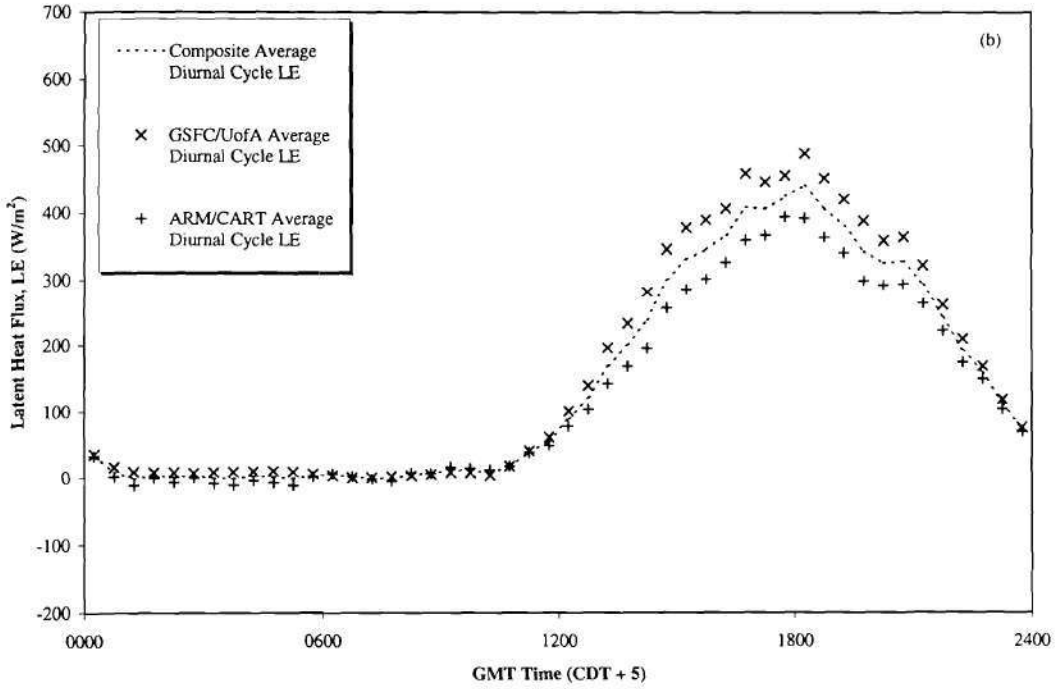

Figure 7 (a) & (b): Average diurnal cycle of surface fluxes of sensible heat flux, H, and latent heat flux, LE, from two eddy correlation systems deployed at the DOE ARM/CART central facility from Day 183 through 197 during SGP97

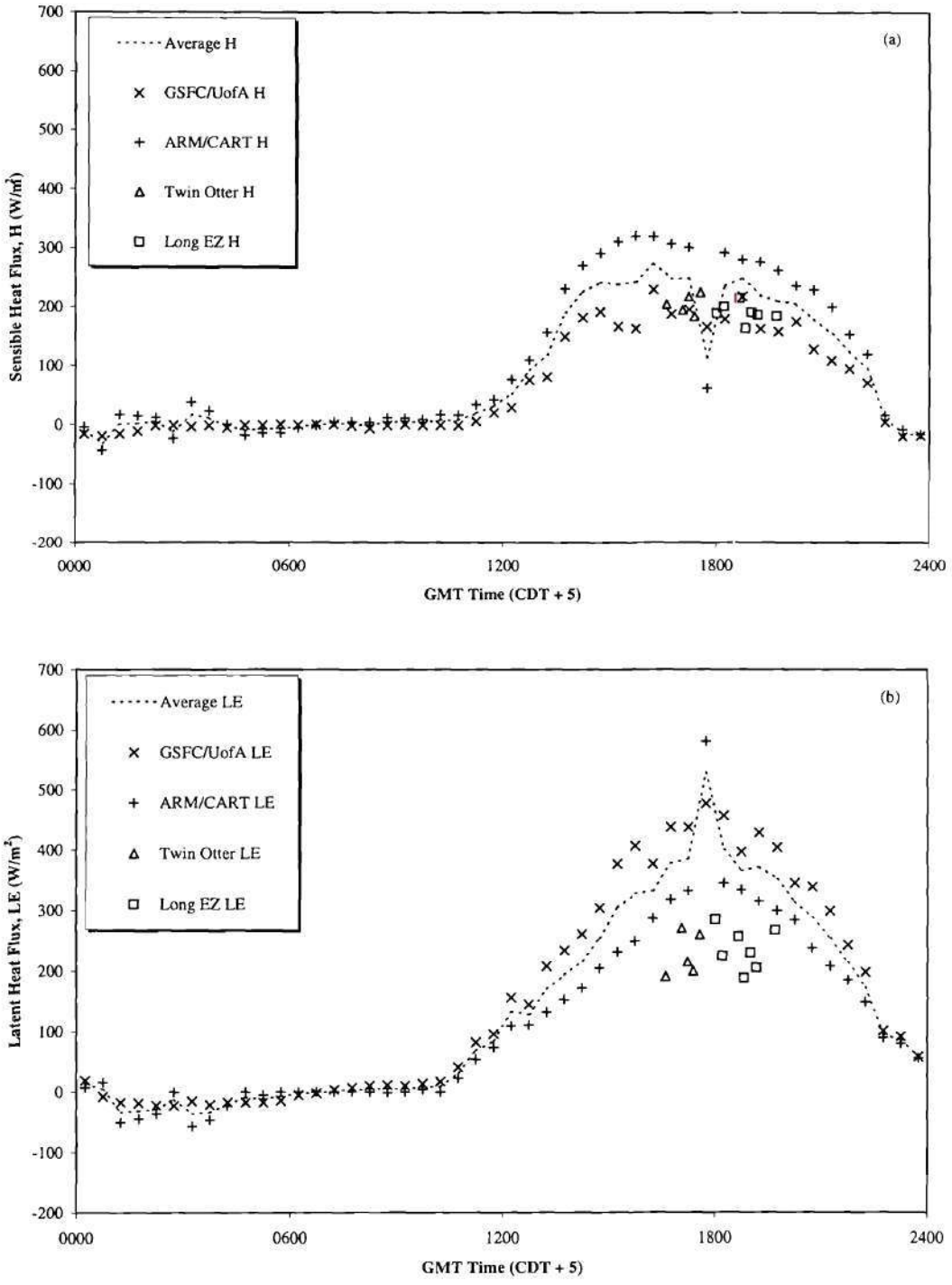

Figure 8 (a) & (b): Day 186 sensible heat flux, H, and latent heat flux, LE, eddy correlation point measured values and Twin-Otter and Long-EZ aircraft regional measured values

Two flux aircraft, the National Research Council (NRC) Twin Otter and NOAA Long EZ, measured regional sensible and latent heat flux at the central facility on July 5, 1997 (Day 186). In order to verify that the combination of the two eddy correlation system point measurements can represent regional surface fluxes, Figure 8 (a) and (b) contain the sensible and latent heat fluxes measured by the two eddy correlation systems and both the Twin Otter and Long EZ. The regional sensible heat fluxes measured by the aircraft show good agreement with the eddy correlation point measurements. However, the regional latent heat fluxes seem to be overestimated by the eddy correlation systems by approximately 25%. This overestimation could be related to the energy closure that is forced on the eddy correlation systems but not on the aircraft data.

Bowen Ratio

A Campbell Scientific Bowen ratio system was located at the ARM/CART central facility throughout SGP97. REBS Q*7.1-L, Campbell Scientific Bowen ratio 023A enclosure with hygrometer and controller, Type E fine-wire thermocouples (TCBR-3), REBS HFT3-L soil heat flux transducers, Campbell Scientific 2X2 (TCAV-L) averaging thermocouple. The Bowen ratio measurements include downward solar radiation, net radiation, ground heat flux, soil temperature, and changes in both temperature and vapor pressure.

After post processing the measured data, the Bowen ratio system was found to have several unidentifiable problems and did not yield accurate estimates of sensible and latent heat flux. The ground heat flux values were also suspect since they were much larger than those measured at the surrounding flux stations. However, the net radiation recorded by the Bowen ratio system compared well with the other flux stations, with a root mean square error of $\pm$ 10 W/m^2 when contrasted with the UWM values.

Quality Control/Procedures

During SGP97, a preliminary in-situ analysis of the collocated tethersonde data and ARM/CART radiosonde data at the central facility indicated good agreement between the measured temperature and humidity vertical profiles. After the field experiment, further analysis between the two datasets revealed a cool and dry bias in the tethersonde data after June 25, 1997 (Day 176), the day that the AIRsonde was replaced (see above). Prior to June 25, the tethersonde temperature and humidity vertical profiles continue to exhibit excellent agreement with the radiosonde data. After June 25, the average dry bulb temperature bias is $\pm$ 2.5 Kelvin and the average specific humidity bias is $\pm$ 5.1 grams per kilogram. Dry bulb temperature (T) is used for comparison between the tethersonde and radiosonde because both instruments directly measure T. With regards to humidity, the tethersonde solves for relative humidity (RH) using T and wet bulb temperature (T_w) while the radiosonde measures RH directly, necessitating the use of specific humidity to evaluate the two instruments.

In an attempt to find a stable bias correction for the tethersonde data, an experiment was performed from July 9-12, 1998 (Day 190 to 193), in which pressure,

temperature, and humidity data were collected using both AIRsondes and a meteorological station. The first AIRsonde again showed good agreement with the surface meteorological data while the second AIRsonde displayed the cool and dry bias again but with different magnitudes from those observed from the SGP97 dataset. Since the bias in the second AIRsonde displayed a different magnitude than the SGP97 bias, another approach was employed to eliminate the tethersonde bias as described below.

The bias correction procedure that was implemented came from a regression analysis in which the tethersonde and radiosonde temperature and humidity vertical profiles were compared. Since the radiosonde has a larger vertical spatial resolution than the tethersonde (10-15 meters), radiosonde dry bulb temperature and specific humidity profiles were first linearly interpolated to the pressure levels of the tethersonde data. The possible predictors for the corrected dry bulb temperature (T_c) and specific humidity (q_c) were the tethersonde measured pressure, dry and wet bulb temperature, and relative humidity, as well as derived potential temperature and specific humidity values.

Dry Bulb Temperature

With both the tethersonde and radiosonde measuring dry bulb temperature directly, the radiosonde dry bulb temperature was chosen as the dependent variable. The best fit came from a simple linear regression that only used one predictor, measured tethersonde dry bulb temperature, as shown below:

$$T_c = 1.82 + 0.994\ T \qquad (1)$$

where T_c is the corrected tethersonde dry bulb temperature in degrees Celsius and T is the measured tethersonde dry bulb temperature in degrees Celsius. This simple linear regression model had an adjusted correlation coefficient of 86.8 and a root mean square error of $\pm$ 1.82 degrees Celsius. Multiple linear regression approaches using other predictors provided no significant improvement over the simple linear regression. Equation (1) was applied to all measured tethersonde data after June 25, 1997 (Day 176).

Specific Humidity

Since the tethersonde uses measured dry and wet bulb temperature to solve for relative humidity while the radiosonde measures relative humidity directly, the radiosonde specific humidity was chosen as the dependent variable eliminating the bias of a relative measure of atmospheric moisture. Attempts were made to correct the tethersonde specific humidity using simple linear regression, multiple linear regression, nonlinear regression, and an artificial neural network. Of these methods, the nonlinear regression approach provided the best results using equation (2) for the June 25, July 14, and July 16, 1997 (Day 176, 195, and 197) tethersonde data:

$$q_c = 16.1 - 0.00973*(T^2) + 0.0328*(T_w^2) - 0.129*(q^2) + 0.00587*(q^3) \qquad (2)$$

and equation (3) for the June 27 to July 6, 1997 (Day 178 to 187), tethersonde data:

$$q_c = 32.7 - 0.203*(T^2) + 0.489*(T_w^2) + 0.821*(q^2) - 0.0273*(RH^2) + 0.00384*(T^3) - 0.016*(T_w^3) - 0.0868*(q^3) + 0.000307*(RH^3) \quad (3)$$

where q_c is the corrected tethersonde specific humidity, T is the measured tethersonde dry bulb temperature, T_w is the measured tethersonde wet bulb temperature, RH is the measured tethersonde relative humidity, and q is the measured tethersonde specific humidity. These equations have an adjusted correlation coefficient of 81.3 and a root mean square error of 1.1 grams per kilogram.

In-situ Conditions

The June 22 to July 17, 1997 (Day 173 to 198) central facility 30-minute precipitation data recorded on the ARM archive (http://www.archive.arm.gov/cgi-bin/arm-archive) and daily gravimetric soil moisture data from the DAAC are presented in Figure 9 (a) and (b), respectively. Figure 9 (a) shows that rain events occurred on June 24, 26, and 30 (Day 175, 177, and 181) and July 10 and 11, 1997 (Day 191 and 192). In Figure 9 (b), there is corresponding increase in soil moisture following each rain event. Following the rain event on June 30 (Day 181), a gradual dry down in soil moisture occurs until the onset of additional precipitation.

Figure 10 contains the 30-minute calculated daytime (1100 to 2400 GMT) Bowen ratios from the eddy correlation systems from July 2 to July 17, 1997 (Day 183 to 198). With the dry down in soil moisture after rain event on June 30 (Day 181), there is a corresponding decrease in latent heat flux shown in the larger Bowen ratio values (with a maximum of ≈ 1.0). After the July 10 (Day 191) rain event, latent heat flux increases causing the smaller Bowen ratio values beginning the next day. The last few days of the experiment had fairly constant daytime Bowen ratios with a maximum of ≈ 0.5.

The 30-minute downward solar radiation and both the 10 and 25 meter infrared thermometer (IRT) surface temperatures from the ARM archive are summarized in Figure 11 (a) and (b). Both the downward solar radiation and surface temperature decrease on July 11 (Day 192), implying an overcast, cooler day. The IRT surface temperatures are used in the surface similarity approach as detailed in Chapter IV.

The tethersonde average wind speed (WS) and inversion heights (Zi) are given in Figures 2.12 (a) and (b) with corresponding inversion and free atmosphere level potential temperature (Θ_i, Θ_{fa}) and specific humidity (q_i, q_{fa}) in Figure 13 (a) and (b). Figure 12 (a) and (b) shows a general decrease in average wind speed as the inversion height increases with the growth of the ABL. Both the average wind speed and inversion level potential temperature follow the decreasing trend in soil moisture during the dry down in Figure 9 (b) and corresponding increase in the Bowen ratio in Figure 10.

In Figure 13 (a) and (b), the free atmosphere is warmer and drier and does not display as much variability as the inversion level values. The difference between the two levels is an indicator of the inversion strength, and therefore entrainment. As the

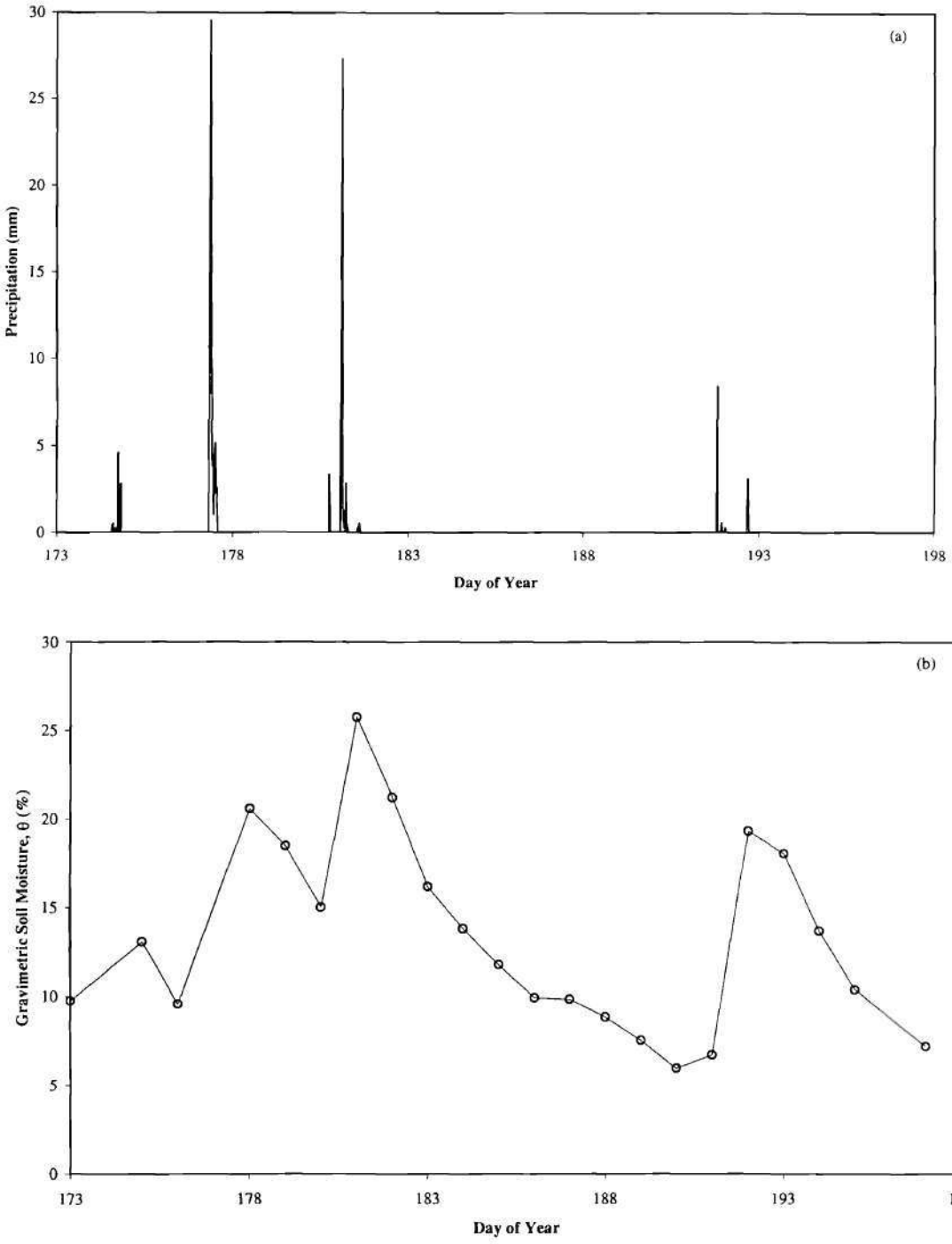

Figure 9 (a) & (b): ARM/CART central facility, CF1, precipitation and site averaged gravimetric soil moisture for Days 173 through 197

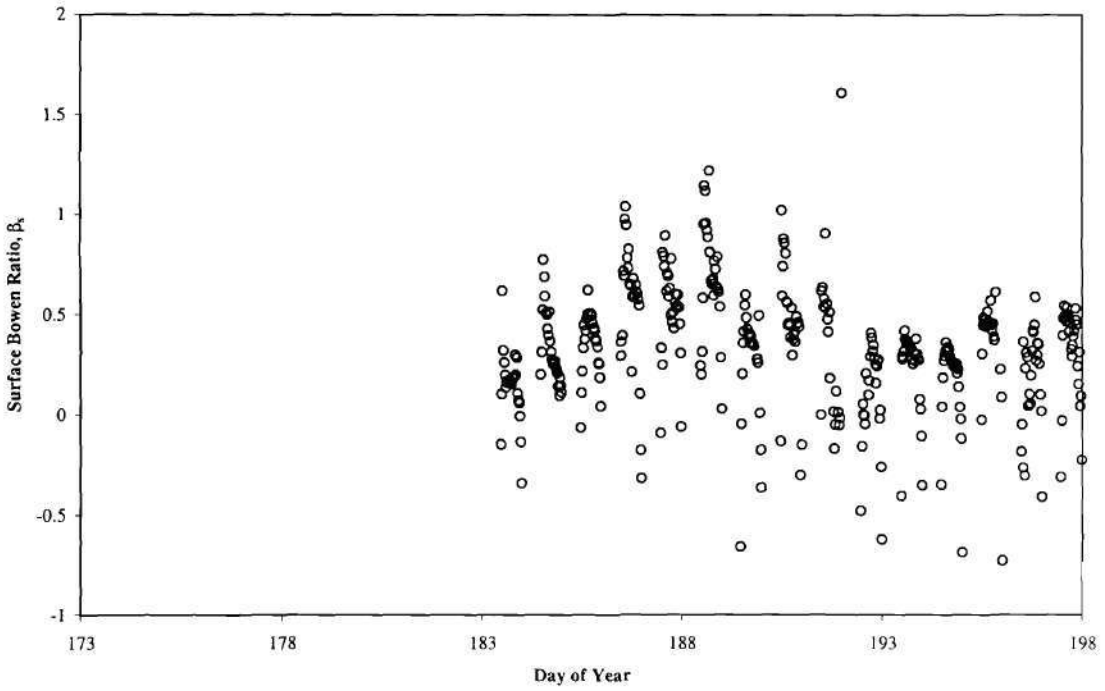

Figure 10: ARM/CART central facility, CF1, daytime (1100 to 2400 GMT) surface Bowen ratios, βs, for Days 183 through 197

difference increases, there should be a corresponding increase in entrainment. Figure 13 (b) demonstrates how the inversion level specific humidity tends to decrease with ABL growth and the soil moisture dry down.

Figure 14 (a) and (b) contains the tethersonde mixed layer average potential temperature (Θ_m) and specific humidity (q_m) values. Similar to the inversion values, the mixed layer average potential temperature follows the decreasing soil moisture during the dry down. As the Bowen ratio decreases in Figure 10, the mixed layer specific humidity tends to decrease due to the lack of latent heat production from the surface.

Analysis

Further analysis of the SGP97 tethersonde profiles by Davis (1999), and Peters-Lidard and Davis (1999) has shown that these data are useful for estimating regional evapotranspiration and sensible heat fluxes over the region surrounding the Central Facility. The reader is referred to these works (see also Appendix B) for further discussion of the theory and issues surrounding the conservation and similarity approaches.

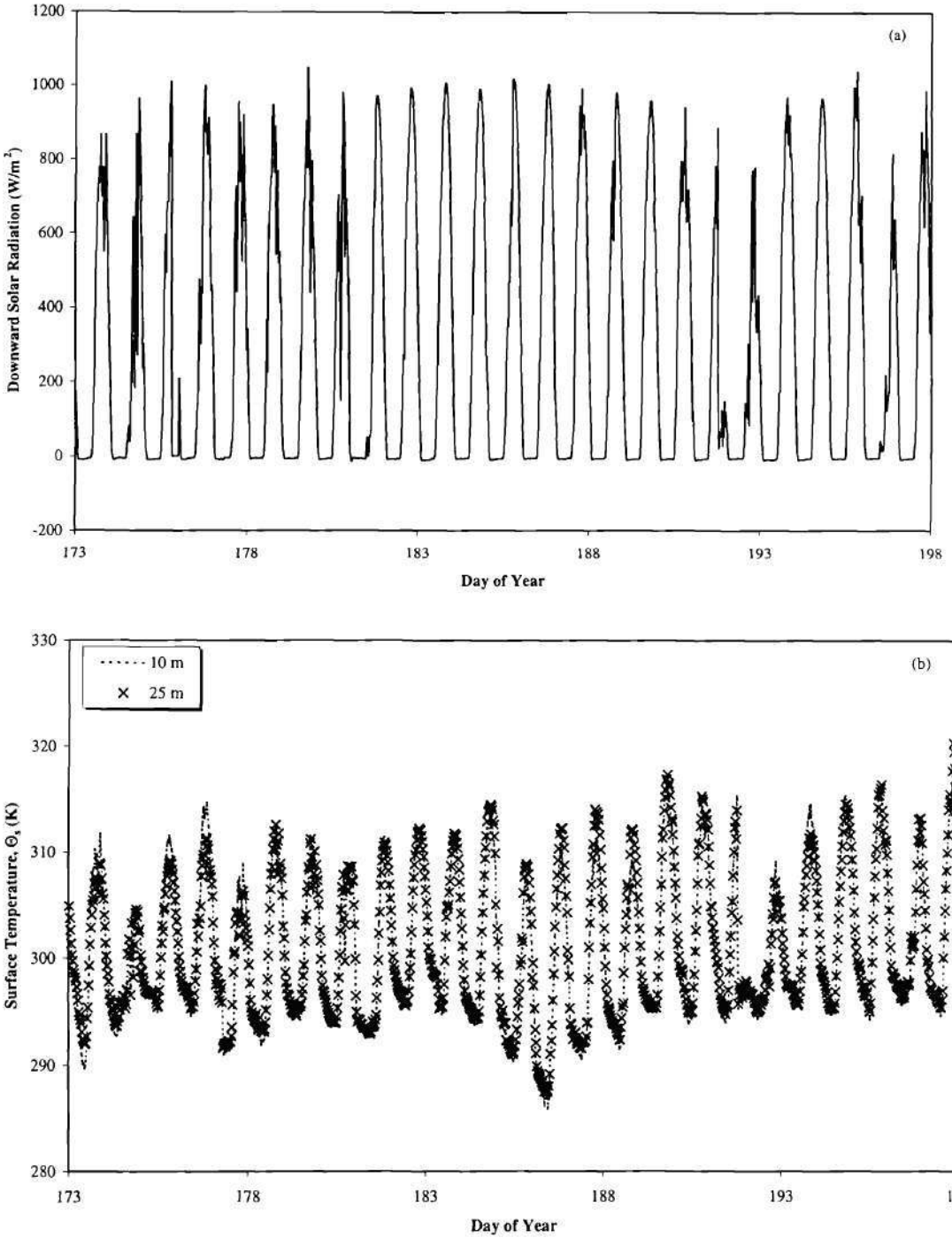

Figure 11 (a) & (b): ARM/CART central facility, CF1, downward solar radiation and surface temperatures, Θ_s, for Days 173 through 197

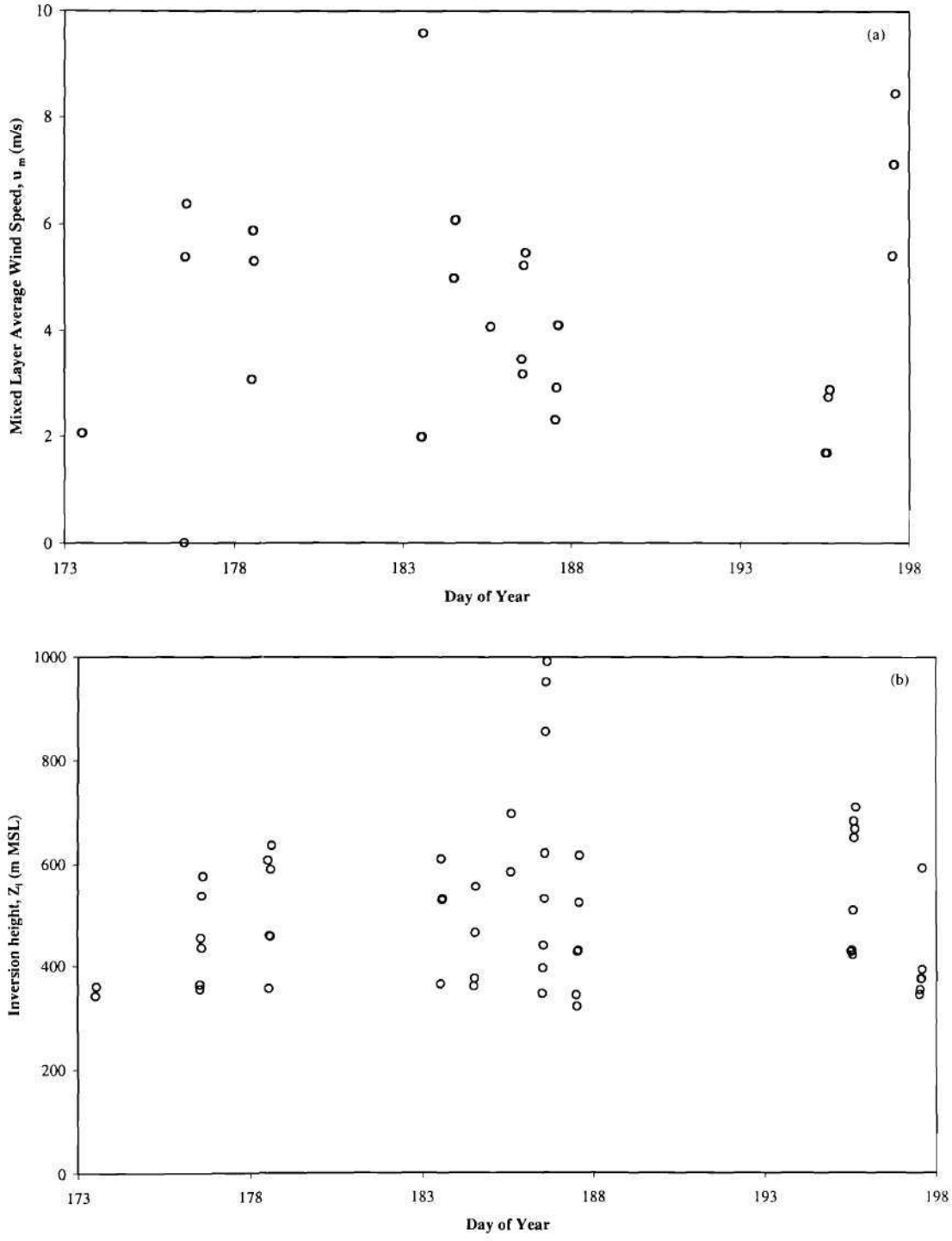

Figure 12 (a) & (b): Tethersonde mixed layer average wind speed, u_m, and measured inversion height, Z_i, for Days 173 through 197

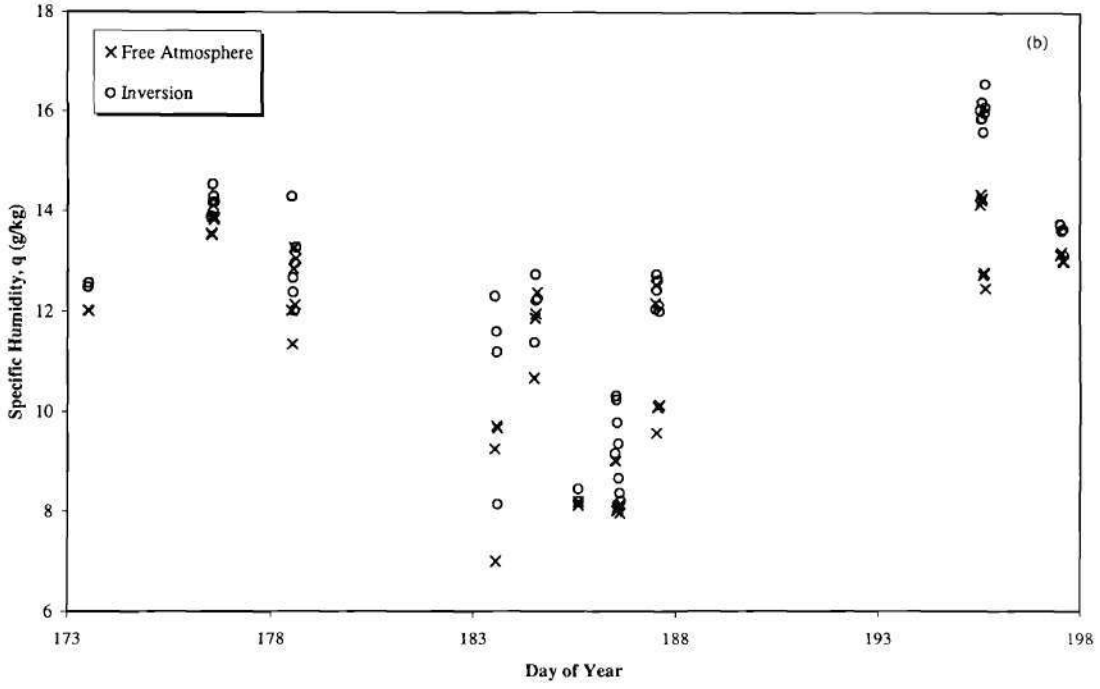

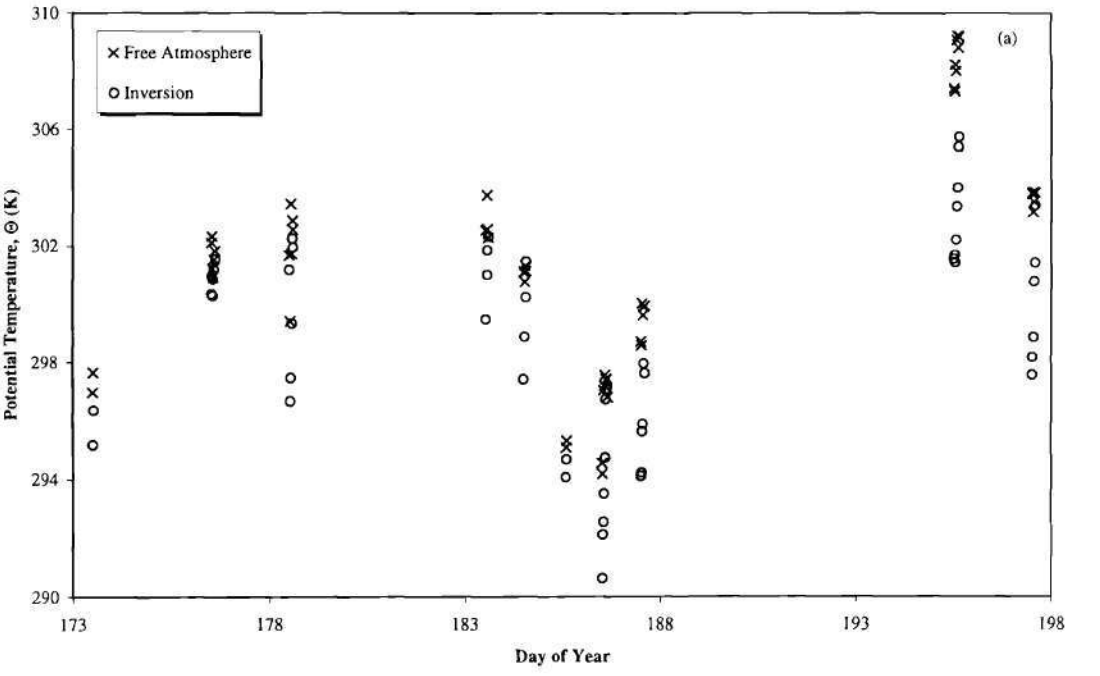

Figure 13 (a) & (b): Tethersonde free atmosphere and inversion potential temperature, Θ_{fa} and Θ_i, and specific humidity, q_{fa} and q_i, for Days 173 through 197

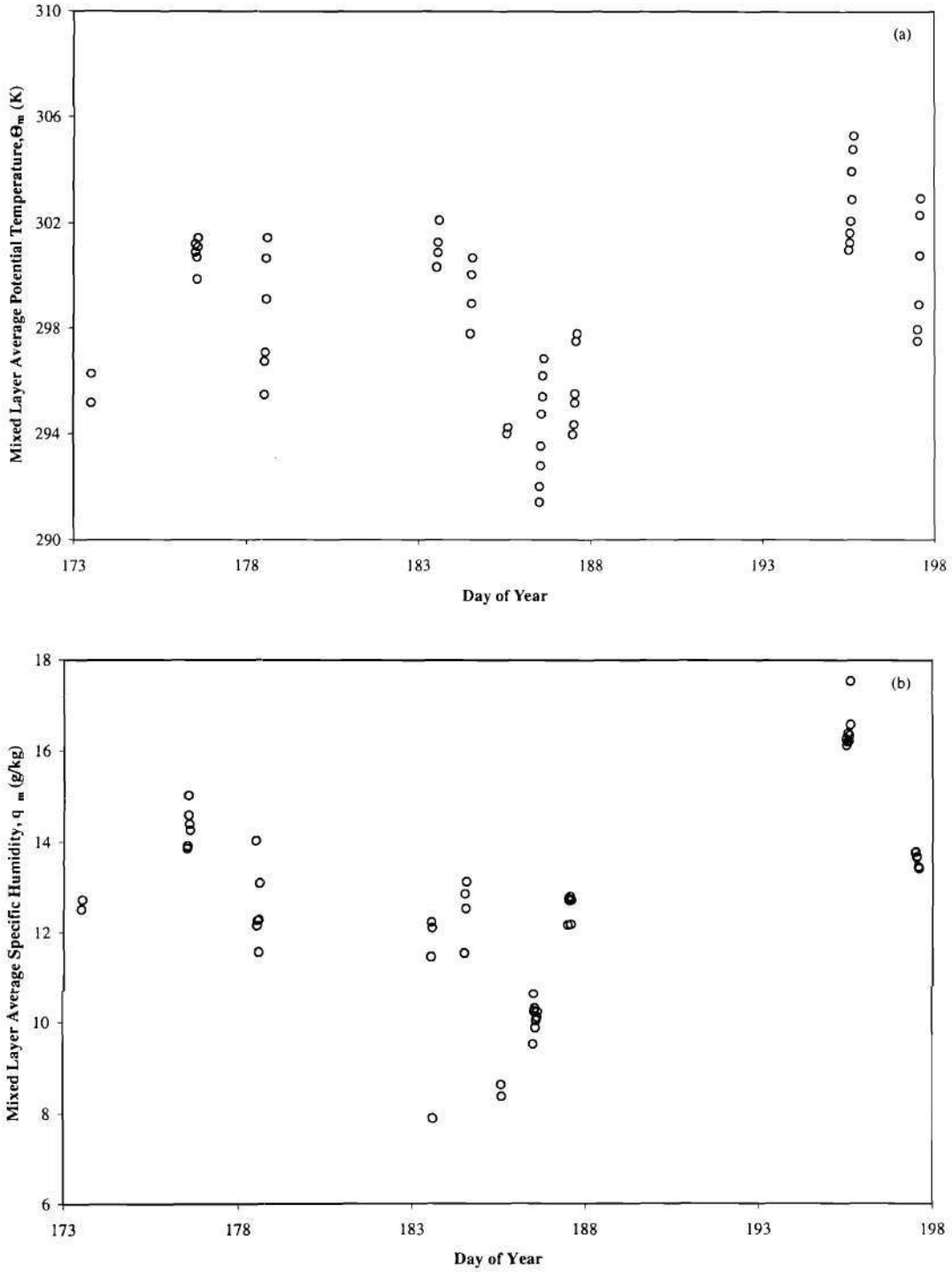

Figure 14 (a) & (b): Tethersonde mixed layer average potential temperature, Θ_m, and specific humidity, q_m, for Days 173 through 197

SUMMARY AND RECOMMENDATIONS

During SGP97, simultaneous tethersonde and radiosonde campaigns provided vertical atmospheric profiles of pressure, temperature, humidity, wind speed and wind direction. The tethersonde could only be deployed in light winds (less than 10 meters per second) which limited operations to sixteen days of flights during SGP97, as listed in Table 2. Each flight consisted of an ascent-descent sequence with ascents beginning at 0700 local time (CDT) and continued hourly through 1100 CDT in the morning hours to capture the ABL growth during the morning transition. During the afternoon, ascents were initiated every one and one-half hours starting at 1230 CDT and lasting until 1700 CDT. Tethersonde thermodynamic and wind data were recorded at a rate of ten seconds, yielding a 2-5 meter vertical resolution with a typical rise rate between 0.2-0.5 meters per second. Due to instrument error, a bias correction derived from regression analysis was applied to the tethersonde data measured after June 25, 1997 (Day 176).

Other supporting ABL measurements in and around the Central Facility included the ARM/CART radiosondes and meteorological stations, several flux stations and one day of flux aircraft flights. The in-situ environmental conditions indicate a long dry down period that is strongly reflected in the tethersonde measurements, including inversion height and inversion and mixed layer average potential temperature and specific humidity.

Further analysis of the SGP97 tethersonde profiles by Davis (1999), and Peters-Lidard and Davis (1999) has shown that these data are useful for estimating regional evapotranspiration and sensible heat fluxes over the region surrounding the Central Facility. The reader is referred to these works (see also Appendix B) for further discussion of the theory and issues surrounding the conservation and similarity approaches. Both methods show good agreement with the measured eddy correlation surface fluxes. However, the ABL conservation approach sensible and latent heat flux estimates have a slightly smaller root mean square error and bias when compared to the ASL similarity approach. ASL similarity theory also requires additional information such as the surface temperature and surface roughness parameters. Overall, the ABL conservation approach is better at estimating regional evapotranspiration, but both approaches are valid and provide good results.

The tethersonde instrument has a high degree of vertical spatial resolution, which should provide better estimates of surface sensible and latent heat flux using the ABL conservation and ASL similarity approaches. However, tethersondes are governed by in-situ advection conditions and the length of the tetherline, limited flights at low to moderate wind locations and surface flux estimates only during the morning growth of the boundary layer. Radiosondes are not affected by the aforementioned limitations and may also be used in the ABL conservation and ASL similarity approaches but do not have the same vertical spatial resolution as the tethersonde.

In future experiments, a combination of tethersonde and radiosonde measurement programs is recommended. The tethersonde operations are quite cost-effective, since the instrument package is re-used for each flight. The only expendables are helium used in

the inflation of the balloon and batteries used to power the antenna and wet bulb fan. Better coordination with and increased frequency of frequent aircraft flights could provide valuable horizontal flux estimates, which in turn could increase the accuracy of the ABL conservation approach for regional flux estimates. Also, flux aircraft campaigns spanning over several days could provide more suitable flux estimates than those provided by surface stations for comparison with regional flux estimates from tethersondes or radiosondes.

REFERENCES

Ball, F. K., Control of inversion height by surface heating, *Quart. J. Roy. Meteor. Soc.*, *86*, 483-494, 1960.

Beljaars, A. C. M., The parameterization of surface fluxes in large-scale models under free convection, *Quart. J. Roy. Meteor. Soc., 121*, 255-270, 1994.

Betts, A. K., FIFE atmospheric boundary layer budget methods, *J. Geophys. Res., 97*, 18,523-18,531, 1992.

Betts, A. K., R. L. Desjardins, and J. I. Macpherson, Budget analysis of the boundary layer grid flights during FIFE 1987, *J. Geophys. Res., 97*, 18,533-18,546, 1992.

Betts, A. K., R. L. Desjardins, J. I. Macpherson, and R. D. Kelly, Boundary-layer heat and moisture budgets from FIFE, *Boundary-Layer Meteorol., 50*, 109-137, 1990.

Brutsaert, W., *Evaporation into the atmosphere*, Kluwer Academic Publishers, Dordrecht, 1982.

Brutsaert, W., Stability correction functions for the mean wind speed and temperature in the unstable surface layer, *Geophys. Res. Lett., 19*, 469-472, 1992.

Brutsaert, W. and W. P. Kustas, Evaporation and humidity profiles for neutral conditions over rugged hilly terrain, *J. Climate Appl. Meteorol., 24*, 915-923, 1985.

Brutsaert, W. and W. P. Kustas, Surface water vapor and momentum fluxes under unstable conditions from a rugged-complex area, *J. Atmos. Sci., 44*, 421-431, 1987.

Brutsaert, W. and M. B. Parlange, The unstable surface layer above forest: regional evapotranspiration and heat flux, *Water Resour. Res., 28*, 3129-3134, 1992.

Brutsaert, W. and M. Sugita, The extent of the unstable Monin-Obukhov layer for temperature and humidity above complex grassland, *Boundary-Layer Meteorol., 51*, 383-400, 1990.

Brutsaert, W. and M. Sugita, Regional surface fluxes from satellite-derived surface temperatures (AVHRR) and radiosonde profiles, *Boundary-Layer Meteorol., 58*, 355-366, 1992a.

Brutsaert, W. and M. Sugita, Regional surface fluxes under nonuniform soil moisture conditions during drying, *Water Resour. Res., 28*, 1669-1674, 1992b.

Businger, J. A., A note on the Businger-Dyer profiles, *Boundary-Layer Meteorol., 42*, 145-151, 1988.

Businger, J. A., J. C. Wyngaard, Y. Izumi, and E. F. Bradley, Flux-profile relationships in the atmospheric surface layer, *J. Atmos. Sci., 28*, 181-189, 1971.

Carson, D. J., The development of a dry inversion-capped convectively unstable boundary layer, *Quart. J. Roy. Meteor. Soc., 99*, 450-467, 1973.

Davis, L. H., 1999: *Evaluation and Verification of Conservation and Similarity Approaches for Estimating Regional Evapotranspiration*. M.S. Thesis, Georgia Institute of Technology, School of Civil and Environmental Engineering, 156 pp. *(summary attached)*

Davis, L. H., C. D. Peters-Lidard, and L. C. Showell, 1999: Estimating Regional Evapotranspiration using an Atmospheric Boundary Layer Conservation Approach. *Preprint volume: 14th Conference on Hydrology, American Meteorological Society, Dallas, Texas.*

Davis, L. H., C. D. Peters-Lidard, and L. C. Showell, 1998: Estimating Regional Evapotranspiration using an Atmospheric Boundary Layer Conservation Approach. *Poster presented at: American Geophysical Union Spring Meeting, 26-29 May 1998, Boston, Mass.*

Driedonks, A. G. M., Models and observations of the growth of the atmospheric boundary layer, *Boundary-Layer Meteorol., 23*, 283-306, 1982.

Dyer, A. J., A review of flux-profile relationships, *Boundary-Layer Meteorol., 7*, 363-372, 1974.

Grachev, A. A. and C. W. Fairall, Dependence of the Monin-Obukhov stability parameter on the bulk Richardson number over the ocean, *J. Appl. Meteorol., 36*, 406-414, 1997.

Hipps, L.E., E. Swiatek, and W. P. Kustas, Interactions between regional surface fluxes and the atmospheric boundary layer over a heterogeneous watershed, *Water Resour. Res.*, *30*, 1387-1392, 1994.

Hogstrom, U. Review of some basic characteristics of the atmospheric surface layer, *Boundary-Layer Meteorol.*, *78*, 215-246, 1996.

Jacobs, J. M., and W. Brutsaert, Momentum roughness and view-angle dependent heat roughness at a Southern Great Plains test-site, *J. Hydrol.*, *211*, 61-68, 1998.

Kader, B. A., and A. M. Yaglom, Mean fields and fluctuation moments in unstably stratified turbulent boundary layers, *J. Fluid Mech.*, *212*, 637-662, 1990.

Kohsiek, W., H. A. R. De Bruin, H. The, and B. Van Der Hurk, Estimation of the sensible heat flux of a semi-arid area using surface radiative temperature measurements, *Boundary-Layer Meteorol.*, *63*, 213-230, 1993.

Kustas, W. P., and W. Brutsaert, Wind profile constants in a neutral atmospheric boundary layer over complex terrain, *Boundary-Layer Meteorol.*, *34*, 35-54, 1986.

Kustas, W. P., and W. Brutsaert, Virtual heat entrainment in the mixed layer over very rough terrain, *Boundary-Layer Meteorol.*, *38*, 141-157, 1987.

Kustas, W. P., L. E. Hipps, and K. S. Humes, Calculation of basin-scale surface fluxes by combining remotely sensed data and atmospheric properties in a semiarid landscape, *Boundary-Layer Meteorol.*, *73*, 105-123, 1994.

Lee, H. N., Improvements of surface flux calculation in the atmospheric surface layer, *J. Appl. Meteorol.*, *36*, 1416-1423, 1997.

Lhomme, J.-P., B. Monteny, and P. Bessemoulin, Inferring regional surface fluxes from convective boundary layer characteristics in a Sahelian environment, *Water Resour. Res.*, *33*, 2563-2569, 1997.

Lilly, D. K., Models of cloud-topped mixed layers under a strong inversion, *Quart. J. Roy. Meteor. Soc.*, *94*, 292-309, 1968.

McNaughton, K. G., and T. W. Spriggs, A mixed-layer model for regional evaporation, *Boundary-Layer Meteorol.*, *34*, 243-262, 1986.

Monin, A. S., and A. M. Obukhov, Basic laws of the turbulent mixing in the ground layer of the atmosphere, *Tr. Geofiz. Inst. Akad. Nauk, S.S.S.R,* No. 24 (151), 163-187, 1954.

Munley, W. G., and L. E. Hipps, Estimation of regional evaporation for a tallgrass prarie from measurements of properties of the atmospheric boundary layer, *Water Resour. Res., 27*, 225-230, 1991.

Parlange, M. B., Eichinger, W. E., and J. D. Albertson, Regional scale evaporation and the atmospheric boundary layer, *Rev. Geophys., 33*, 99-124, 1995.

Peters-Lidard, C. D. and L. H. Davis, 1999: Regional Flux Estimation in a Convective Boundary Layer Using a Conservation Approach. *Submitted to Journal of Hydrometeorology. (attached)*

Qualls, R. J. W. Brutsaert, and W. P. Kustas, Near-surface air temperature as substitute for skin temperature in regional surface flux estimation, *J. Hydrol., 143*, 381-393, 1993.

Sellers, P. T., S. O. Los, C. J. Tucker, C. O. Justice, D. A. Dazlich, G. J. Collatz, and D. A. Randall, A revised land surface parameterization (SIB2) for atmospheric GCMs. Part II: the generation of global fields of terrestrial biophysical parameters from satellite data, *J. Climate, 9*, 706-737, 1996.

Stull, R. B., *An Introduction to Boundary Layer Meteorology*, Kluwer Academic Publishers, Dordrecht, 1988.

Stull, R. B., A convective transport theory for surface fluxes, *J. Atmos. Sci., 51*, 3-22, 1994.

Sugita, M., and W. Brutsaert, Wind velocity measurements in the neutral boundary layer above hilly prarie, *J. Geophys. Res., 95*, 7617-7624, 1990a.

Sugita, M., and W. Brutsaert, Regional surface fluxes from remotely sensed skin temperature and lower boundary layer measurements, *Water Resour. Res., 26*, 2937-2944, 1990b.

Sugita, M., and W. Brutsaert, Daily evaporation from lower boundary layer profiles measured with radiosondes, *Water Resour. Res., 27*, 745-752, 1991.

Sugita, M., T. Hiyama, N. Endo, and S.-F. Tian, Flux determination over a smooth surface under strongly unstable conditions, *Boundary-Layer Meteorol.*, *73*, 145-158, 1995.

Sugita, M., T. Hiyama, and I. Kayane, How regional are the regional fluxes obtained from lower atmospheric boundary layer data?, *Water Resour. Res.*, *33*, 1437-1445, 1997.

Swiatek, E., Estimating regional surface fluxes from measured properties of the atmospheric boundary layer in a semiarid ecosystem, M. S. Thesis, Utah State University, Logan, 1992.

Tennekes, H., A model for the dynamics of the inversion above a convective boundary layer, *J. Atmos. Sci.*, *30*, 558-567, 1973.

Tennekes, H, and A. G. M. Driedonks, Basic entrainment equations for the atmospheric boundary layer, *Boundary-Layer Meteorol.*, *20*, 515-531, 1981.

Wieringa, J., Representative roughness parameters for homogeneous terrain, *Boundary-Layer Meteorol.*, *63*, 323-363, 1993.

APPENDIX

A. Detailed tethersonde flight summary statistics

Table A.1: Inversion height, Zi, pressure, Pi, mixed layer average wind speed, um, and direction, udir, for tethersonde flights

DOY	GMT	a (ascent) / d (descent)	Z_i (m MSL)	P_i (mb)	u_m (m/s)	u_{dir} (degrees)
173	1207	A	342	972	2.1	45
173	1235	D	360	970	2.1	45
176	1238	A	355	970	0.0	50
176	1247	D	364	969	0.0	50
176	1320	A	454	959	5.4	186
176	1341	D	435	961	5.4	186
176	1408	A	537	951	6.4	220
176	1436	D	577	946	6.4	220
178	1205	A	608	942	3.1	145
178	1231	D	356	970	3.1	145
178	1300	A	459	960	5.9	207
178	1336	D	458	960	5.9	207
178	1401	A	590	946	5.3	179
178	1428	D	636	941	5.3	179
183	1240	A	365	967	2.0	264
183	1321	D	611	940	2.0	264
183	1346	A	528	949	9.6	33
183	1425	D	531	948	9.6	33
184	1204	A	361	966	5.0	140
184	1237	D	376	965	5.0	140
184	1305	A	464	956	6.1	177
184	1333	D	557	946	6.1	177
185	1410	A	585	949	4.1	277
185	1428	D	697	936	4.1	277
186	1213	A	346	977	3.5	159
186	1242	D	396	970	3.5	159
186	1301	A	440	966	3.2	143
186	1331	D	531	955	3.2	143
186	1401	A	622	946	5.2	160
186	1430	D	857	919	5.2	160

Table A.1 (cont.): Inversion height, Zi, pressure, Pi, mixed layer average wind speed, um, and direction, udir, for tethersonde flights

DOY	GMT	a (ascent) / d (descent)	Z_i (m MSL)	P_i (mb)	u_m (m/s)	u_{dir} (degrees)
186	1501	A	952	909	5.5	166
186	1530	D	991	904	5.5	166
187	1205	A	344	973	2.3	140
187	1234	D	322	976	2.3	140
187	1300	A	428	965	2.9	164
187	1329	D	430	964	2.9	164
187	1400	A	523	955	4.1	191
187	1429	D	618	944	4.1	191
195	1206	a	429	962	1.7	109
195	1235	d	432	961	1.7	109
195	1300	a	423	963	1.7	110
195	1327	d	509	954	1.7	110
195	1400	a	684	935	2.7	66
195	1428	d	652	939	2.7	66
195	1500	a	669	937	2.9	108
195	1525	d	711	933	2.9	108
197	1208	a	345	973	5.4	158
197	1227	d	354	972	5.4	158
197	1300	a	375	970	7.1	180
197	1328	d	376	969	7.1	180
197	1400	a	394	969	8.4	186
197	1424	d	594	946	8.4	186

Table A.2: Tethersonde potential temperature found at the inversion height, Θ_i, start of the free atmosphere, Θ_{fa}, and profile average, Θ_m

DOY	GMT	a (ascent) / d (descent)	Θ_i (K)	Θ_{fa} (K)	Θ_m (K)
173	1207	a	295.2	297.0	295.2
173	1235	d	296.4	297.7	296.3
176	1238	a	300.4	302.1	300.9
176	1247	d	301.0	302.3	301.2
176	1320	a	300.3	301.2	299.9
176	1341	d	300.9	300.9	300.7
176	1408	a	301.2	301.5	301.1
176	1436	d	301.6	301.8	301.4
178	1205	a	301.2	301.7	295.5
178	1231	d	296.7	299.4	296.8
178	1300	a	297.5	303.5	297.1
178	1336	d	299.3	301.7	299.1
178	1401	a	302.3	302.9	300.6
178	1428	d	302.0	302.6	301.4
183	1240	a	299.5	302.6	300.3
183	1321	d	301.0	303.8	300.9
183	1346	a	301.9	302.6	301.3
183	1425	d	302.3	302.3	302.1
184	1204	a	297.4	301.1	297.8
184	1237	d	298.9	300.8	299.0
184	1305	a	300.3	301.3	300.1
184	1333	d	301.5	301.2	300.7
185	1410	a	294.1	295.1	294.0
185	1428	d	294.7	295.3	294.2
186	1213	a	290.6	294.6	291.4
186	1242	d	292.1	294.2	292.0
186	1301	a	292.6	297.1	292.8
186	1331	d	293.5	297.2	293.5
186	1401	a	294.8	297.6	294.7
186	1430	d	296.8	297.4	295.4
186	1501	a	297.1	297.4	296.2
186	1530	d	297.2	296.8	296.9

Table A.2 (cont.): Tethersonde potential temperature found at the inversion height, Θ_i, start of the free atmosphere, Θ_{fa}, and profile average, Θ_m

DOY	GMT	a (ascent) / d (descent)	Θ_i (K)	Θ_{fa} (K)	Θ_m (K)
187	1205	a	294.1	298.7	294.0
187	1234	d	294.2	298.6	294.4
187	1300	a	295.7	300.0	295.2
187	1329	d	295.9	299.6	295.5
187	1400	a	298.0	299.9	297.6
187	1429	d	297.6	300.0	297.8
195	1206	a	301.6	307.4	301.0
195	1235	d	301.7	307.3	301.2
195	1300	a	301.5	308.2	301.6
195	1327	d	302.2	308.0	302.1
195	1400	a	303.4	309.1	302.9
195	1428	d	304.0	309.2	304.0
195	1500	a	305.4	308.8	304.8
195	1525	d	305.8	309.2	305.3
197	1208	a	297.6	303.8	297.5
197	1227	d	298.2	303.9	298.0
197	1300	a	298.9	303.2	298.9
197	1328	d	300.8	303.5	300.8
197	1400	a	301.4	303.9	302.3
197	1424	d	303.4	303.9	302.9

Table A.3: Tethersonde specific humidity found at the inversion height, q_i, start of the free atmosphere, q_{fa}, and profile average, q_m

DOY	GMT	a (ascent) / d (descent)	q_i (g/kg)	q_{fa} (g/kg)	q_m (g/kg)
173	1207	a	12.5	12.0	12.5
173	1235	d	12.6	12.0	12.7
176	1238	a	13.9	13.6	13.9
176	1247	d	13.9	13.5	13.9
176	1320	a	14.5	13.9	15.0
176	1341	d	14.2	14.1	14.6
176	1408	a	14.3	13.8	14.4
176	1436	d	14.2	13.9	14.3
178	1205	a	14.3	12.0	14.0
178	1231	d	12.7	11.4	12.2
178	1300	a	12.4	12.9	12.3
178	1336	d	12.0	13.3	11.6
178	1401	a	13.0	12.1	12.3
178	1428	d	13.3	13.1	13.1
183	1240	a	12.3	9.3	11.5
183	1321	d	11.6	7.0	12.2
183	1346	a	11.2	9.7	12.1
183	1425	d	8.2	9.7	7.9
184	1204	a	11.4	10.7	11.6
184	1237	d	12.8	11.9	12.9
184	1305	a	12.2	12.0	12.5
184	1333	d	12.3	12.4	13.1
185	1410	a	8.5	8.1	8.6
185	1428	d	8.2	8.2	8.4
186	1213	a	9.2	9.0	9.5
186	1242	d	10.3	9.0	10.6
186	1301	a	10.2	8.0	10.2
186	1331	d	9.8	8.1	10.3
186	1401	a	9.4	8.1	9.9
186	1430	d	8.7	8.1	10.0
186	1501	a	8.4	8.0	10.1
186	1530	d	8.2	8.2	10.2

Table A.3 (cont.): Tethersonde specific humidity found at the inversion height, q_i, start of the free atmosphere, q_{fa}, and profile average, q_m

DOY	GMT	a (ascent) / d (descent)	q_i (g/kg)	q_{fa} (g/kg)	q_m (g/kg)
187	1205	a	12.1	12.2	12.2
187	1234	d	12.8	12.5	12.8
187	1300	a	12.4	9.6	12.7
187	1329	d	12.6	10.1	12.8
187	1400	a	12.1	10.1	12.2
187	1429	d	12.0	10.1	12.7
195	1206	a	16.0	14.1	16.3
195	1235	d	15.9	14.4	16.1
195	1300	a	15.9	14.2	16.2
195	1327	d	16.2	14.3	16.4
195	1400	a	15.6	12.7	16.2
195	1428	d	16.0	12.8	16.3
195	1500	a	16.1	12.8	16.6
195	1525	d	16.6	12.5	17.5
197	1208	a	13.8	13.1	13.8
197	1227	d	13.7	13.1	13.8
197	1300	a	13.6	13.2	13.7
197	1328	d	13.6	13.0	13.7
197	1400	a	13.7	13.0	13.5
197	1424	d	13.1	13.0	13.4

B. Publications and Presentations Resulting from this Research

Davis, L. H., 1999: *Evaluation and Verification of Conservation and Similarity Approaches for Estimating Regional Evapotranspiration*. M.S. Thesis, Georgia Institute of Technology, School of Civil and Environmental Engineering, 156 pp. *(summary attached)*

Davis, L. H., C. D. Peters-Lidard, and L. C. Showell, 1999: Estimating Regional Evapotranspiration using an Atmospheric Boundary Layer Conservation Approach. *Preprint volume: 14th Conference on Hydrology, American Meteorological Society, Dallas, Texas.*

Davis, L. H., C. D. Peters-Lidard, and L. C. Showell, 1998: Estimating Regional Evapotranspiration using an Atmospheric Boundary Layer Conservation Approach. *Poster presented at: American Geophysical Union Spring Meeting, 26-29 May 1998, Boston, Mass.*

Peters-Lidard, C. D. and L. H. Davis, 1999: Regional Flux Estimation in a Convective Boundary Layer Using a Conservation Approach. *Submitted to Journal of Hydrometeorology. (attached)*

SUMMARY: Davis, L. H., 1999: Evaluation and Verification of Conservation and Similarity Approaches for Estimating Regional Evapotranspiration. *M.S. Thesis, Georgia Institute of Technology, School of Civil and Environmental Engineering, 156 pp.*

In this study, tethersonde data collected during the 1997 Southern Great Plains Experiment (SGP97) at the ARM/CART Central Facility in Billings, Oklahoma is used to evaluate and verify Atmospheric Boundary Layer (ABL) conservation and Monin-Obukhov Atmospheric Surface Layer (ASL) similarity approaches for estimating regional evapotranspiration in the form of latent heat flux. Comparisons with independent direct measures of sensible and latent heat fluxes from local eddy correlation systems are used to verify the accuracy of each approach.

In the ABL conservation approach, reasonable regional latent heat fluxes were found by calculating sensible heat flux directly and estimating latent heat flux as a residual from the surface energy balance. Direct estimates of latent heat flux had much larger root mean square errors and bias than the latent heat fluxes calculated as a residual. The ABL conservation approach is highly sensitive to both parameterizations and direct estimates of advection and entrainment. Four advection parameterizations were applied and all provided reasonable results within the standard deviation error of the eddy correlation systems. However, the tethersonde data could only be collected during periods of low to moderate winds, limiting the influence of advection in this approach.

An attempt at modeling entrainment as a constant value during the morning growth of the ABL revealed good agreement with the surface fluxes. Direct estimates of the entrainment flux using empirical equations yielded similar results.

Monin-Obukhov ASL similarity theory also found reasonable regional latent heat flux estimates by solving for sensible heat first and latent heat flux as a residual. Derived surface roughness parameters were consistent with previously determined values and require measurements of the surface potential temperature. The two sets of stability correction functions utilized both demonstrated good agreement with the surface sensible and latent heat fluxes. However, the Businger-Dyer method had a slightly lower root mean square error and bias than the Brutsaert method in the estimation of momentum flux.

MANUSCRIPT. Peters-Lidard, C. D. and L. H. Davis, 1999: Regional Flux Estimation in a Convective Boundary Layer Using a Conservation Approach. Submitted to Journal of Hydrometeorology.

Regional Flux Estimation in a Convective Boundary Layer Using a Conservation Approach

Christa D. Peters-Lidard[1] and Luke H. Davis

School of Civil and Environmental Engineering

Georgia Institute of Technology

Atlanta, Georgia

Submitted to the *Journal of Hydrometeorology*, February, 1999

Revised August, 1999

[1] Corresponding Author Address: Dr. Christa Peters-Lidard, Assistant Professor, School of Civil and Environmental Engineering, Georgia Institute of Technology, 790 Atlantic Drive, Atlanta, GA 30332-0355, ph: 404-894-5190, fax: 404-894-2677, email: cpeters@ce.gatech.edu.

Abstract

During the Southern Great Plains 1997 (SGP97) Hydrology Experiment, a tethersonde system was deployed at the U.S. Department of Energy's Atmospheric Radiation Measurement/Cloud and Radiation Testbed (ARM/CART) Central Facility. Additional measurements included several surface flux stations at the Central Facility and radiosondes at the ARM/CART Central and Boundary Facilities. Combined, these data support an examination of regional flux estimates obtained via the Atmospheric Boundary Layer (ABL) conservation approach. Because the tethersonde was successfully deployed only under light to moderate wind conditions, the effects of advection on estimation of regional fluxes are found to be generally small. Consistent with previous studies, direct estimation of the sensible heat flux yields more accuracy than direct estimation of the latent heat flux. Using available energy measured at surface flux stations along with the direct sensible heat flux estimates yields latent heat estimates of similar accuracy to those obtained for the sensible heat flux. Finally, it is observed that variability in the entrainment parameter exhibits a considerable diurnal cycle, presumably related to the interplay between buoyant and shear production of turbulent kinetic energy (TKE) near the entrainment zone.

1. Introduction

Estimation of regional fluxes of heat and moisture is an issue with crucial importance in numerical weather prediction, climate, agriculture and water resources management. Two classes of approaches have been employed to provide these estimates with varying degrees of success. The first approach is based on extensions to Monin-Obukhov surface layer similarity theory (e.g. Brutsaert and Kustas, 1987; Sugita and Brutsaert, 1990; Brutsaert and Parlange, 1992; Munley and Hipps, 1991; Swiatek, 1992; Sugita et al., 1997). As recently discussed by Sugita et al. (1997), the "region" associated with flux estimation using this method is of order 1-10 km^2, and application of this approach is hindered by difficulties in specifying the appropriate surface temperature as well as time-dependent scalar roughness (z_{oh}).

The second type of approach to regional flux estimation is the atmospheric boundary layer (ABL) conservation or budget method (e.g. McNaughton and Spriggs, 1986; Munley and Hipps, 1991; Swiatek, 1992; Hipps et al., 1994; Kustas et al., 1994; Lhomme et al., 1997). These methods are more data-intensive than similarity methods, since they require two successive atmospheric soundings through the entrainment zone to obtain one flux estimate. In addition, the ABL conservation method has been shown to be sensitive to the estimated inversion height (Munley and Hipps, 1991), as well as representations of advection (Swiatek, 1992; Hipps et al., 1994), and entrainment (de Bruin, 1983; McNaughton and Spriggs, 1986).

In this work, we focus on the ABL conservation approach to estimate regional fluxes of heat and moisture in the convective boundary layer. In particular, we examine the currently available approximations for advection and entrainment, since the representation of these

processes is crucial to the accuracy of regional flux estimates. In the following section, ABL conservation theory is reviewed with emphasis on the representation of advection and entrainment. In section 3, we describe the datasets used in this study, and this is followed by an analysis of the effects of advection on regional heat flux estimation. Section 5 presents an examination of the diurnal cycle of entrainment and the final section presents our conclusions.

2. Theoretical Considerations

Current ABL conservation theory is largely based upon the work of Betts (1973), Carson (1973) and Tennekes (1973), who focused on inversion capped convective boundary layer models with several simplifying assumptions to allow the solution of the conservation equations with limited data. The reader is referred to Stull (1988) and Betts (1992) for more details on the development, as only the simplified forms are given here.

Both conservation equations are Reynolds averaged and simplified by neglecting molecular diffusion, sources and sinks[2], and horizontal flux divergence. In addition, the x coordinate is aligned with the mean wind and the temperature gradient is assumed in the same direction. The simplified conservation of heat equation is:

$$\frac{\partial \overline{\theta}}{\partial t} + \overline{u}\frac{\partial \overline{\theta}}{\partial x} + \overline{w}\frac{\partial \overline{\theta}}{\partial z} = -\frac{\partial \overline{w'\theta'}}{\partial z} \qquad (1)$$

where $\overline{w'\theta'}$ is the kinematic heat flux. The conservation of moisture equation reduces to a similar form in terms of the kinematic moisture flux $\overline{w'q'}$:

[2] It is important to note that sources and sinks may not always be negligible (e.g. radiation flux divergence) as discussed by Kustas and Brutsaert (1987b). We assume that they are negligible in the early morning hours.

$$\frac{\partial \overline{q}}{\partial t} + \overline{u}\frac{\partial \overline{q}}{\partial x} + \overline{w}\frac{\partial \overline{q}}{\partial z} = -\frac{\partial \overline{w'q'}}{\partial z} \tag{2}$$

As Betts (1992) discusses, the presence of a well-mixed layer from the surface to the base of the capping inversion at a height Z_i, allows further simplification of the conservation equations by defining mixed layer averages. Betts brings out an important point regarding the representation of entrainment in mixed layer models; namely, the integration of (1) yields an equation of the form:

$$\overline{\rho}_m Z_i \frac{\partial \overline{\theta}_m}{\partial t} + \overline{\rho}_m Z_i \overline{u}_m \frac{\partial \overline{\theta}_m}{\partial x} = (F_{s\theta} - F_{i\theta}) \tag{3}$$

where the overbar represents Reynolds averaged quantities, the subscript "m" denotes a density-weighted mixed layer average, the surface heat flux is $F_{s\theta} = \overline{\rho w'\theta'}_s$, the inversion level flux is $F_{i\theta} = \overline{\rho w'\theta'}_i + \overline{\rho} W_e(\theta_i - \overline{\theta}_m)$, and $W_e = (\partial Z_i / \partial t - \overline{w}_i)$. As Betts (1992) points out, the $\partial Z_i / \partial t$ term arises in performing a layer average to a moving boundary (see also Kustas and Brutsaert, 1987b), and $\overline{w}_i$ arises from the integration of the subsidence term in (1). Generally, $(\theta_i - \overline{\theta}_m)$ should be small, but the inclusion of this term represents the stratification within the ABL below the inversion base. Note also that if subsidence can be neglected, the growth of the boundary layer due to entrainment reduces to $W_e = \partial Z_i / \partial t$.

It is important to clarify the relationship between (3) and variants of the McNaughton and Spriggs (1986) model, which has been applied by various authors mentioned above. In these approaches, the inversion level flux $F_{i\theta}$ is represented assuming a jump at the inversion

$$F_{i\theta} = (\theta_{fa} - \overline{\theta}_m)\frac{\partial Z_i}{\partial t} \tag{4}$$

where θ_{fa} is the potential temperature at the top of the inversion or entrainment zone (i.e. the "free atmosphere") and we note that $\theta_{fa} \neq \theta_i$. In (4) we have replaced the typical notation using the subscript "fa" rather than "s" so as to avoid confusion with surface values. An important observation regarding (4) is that approaches based upon this approximation rely not only upon estimation of inversion base heights, but also on identification of the proper "free atmosphere" temperature in the inversion flux estimate, which is typically based on the lapse rate γ.

a. Entrainment

Early work on mixed layer budget methods recognized the importance of entrainment in the development of the atmospheric boundary layer. The simplest closure assumption to yield the solution to (3) given two atmospheric profiles is that the inversion level flux is proportional to the surface flux, viz.

$$F_{i\theta} = -A_R F_{s\theta} \tag{5}$$

where A_R is known as the entrainment parameter and is assumed to vary from 0 to 1. Carson (1973) recognized that the entrainment parameter should vary over the course of a day, but found acceptable results with a constant value of 0.5 several hours after the time of maximum surface heating. Values between 0.1 and 0.3 have been regarded as acceptable for strongly convective conditions over flat terrain, and the midpoint, 0.2, has been generally regarded as a "standard" value (e.g. Tennekes, 1973; Stull, 1988). However, various field experiments have revealed significant variation in A_R. Brutsaert (1987) found values ranging from 0.4 to 0.6 in a weakly convective environment. Over rough terrain, Kustas and Brutsaert (1987b) found A_R=0.53$\pm$0.3

for afternoon values and Betts' et al. (1990, 1992) analysis of the FIFE data indicated values closer to 0.4. Tennekes (1973) and Driedonks (1982) also suggested a more complex model of the form:

$$-\overline{w'\theta'}_i = a(\overline{w'\theta'}_s) + b\frac{u_*^3 T}{gZ_i} \tag{6}$$

where u_* is the shear velocity, T is temperature, and g is the acceleration of gravity. The constants a=0.2 and b=2.5 were suggested by Tennekes (1973), and b=5 was suggested by Driedonks (1982). Kustas and Brutsaert (1987b) extended (6) to account for virtual heat flux at the inversion and found a=0.17$\pm$0.13 and b=3.97$\pm$1.59.

b. Advection

Horizontal advection appears as the second term in (1) and (2). Various authors have shown that horizontal advection is important in a volumetric budget model of the ABL (Betts et al., 1990; Swiatek, 1992; and Hipps et al., 1994), although its importance depends on the synoptic situation (Lhomme et al., 1997). Advection has been estimated from synoptic charts (e.g. Kustas and Brutsaert, 1987a) or directly from aircraft data (e.g. Betts et al., 1992).

A simplified advection estimate for the conservation of heat equation proposed by Swiatek (1992) and utilized by Hipps et al., (1994) is:

$$h\overline{u}_m\frac{\partial\overline{\theta}_m}{\partial x} = -h\frac{\partial\theta_{fa}}{\partial t} \tag{7}$$

where h is the height of the inversion (defined not as the inversion base, but closer to the middle of the entrainment zone according to the shape of the potential temperature profile), and θ_{fa} is

the potential temperature in the "free atmosphere" at the top of the inversion. An analogous form of (7) is given for the conservation of moisture equation. It is noted that (7) is meant to be a rather crude approximation of advective flux given the inherent difficulties associated with its direct estimation.

Given two successive soundings, we may solve (3) for $F_{s\theta} = \overline{\rho w'\theta'}_s$ subject to entrainment estimates (4), (5), or (6) and advection estimates via (7) or direct measurements if available. While the technique is conceptually straightforward, a major difficulty in the method is that both advection and entrainment processes are difficult to specify, and uncertainties in both terms impossible to uniquely quantify. Investigation of these uncertainties is one of the major objectives of this work

The surface sensible and latent heat fluxes in [Wm^{-2}] are then estimated from the kinematic fluxes:

$$H_s = \rho C_p \overline{w'\theta'}_s \tag{8}$$

$$LE_s = \rho L_v \overline{w'q'}_s \tag{9}$$

where H is the sensible heat flux, ρ is the density of air, C_p is the specific heat at constant pressure, LE is the latent heat flux, and L_v is the latent heat of vaporization. The latent heat flux may also be estimated as a residual from the energy balance, given the available energy $(R_n\text{-}G)$ and an estimate of sensible heat flux from (8):

$$LE_s = (R_n - G) - H_s \tag{10}$$

3. Data

a. Tethersonde

An Atmospheric Instrumentation Research (AIR)-3A tethersonde system was deployed by the authors at the DOE Atmospheric Radiation Measurement/Cloud and Radiation Testbed (ARM/CART) Central Facility near Lamont, Oklahoma during the Southern Great Plains 1997 (SGP97) Hydrology Experiment (Jackson, 1997). The SGP97 experimental domain is shown in Figure 1, and Figure 2 illustrates the ARM/CART Central Facility, including the exact location of the tethersonde and other data used in this work. The tethersonde, provided by NOAA's National Severe Storms Laboratory (NSSL), was available throughout the experiment (June 18,1997 until July 17, 1997), but was only able to successfully deploy under light to moderate wind conditions so that a total of sixteen days of flights were completed during SGP97 (Table 1). As shown in the last column of Table 1, each day of flights were ranked based on the criteria in Table 2. This ranking process yielded 5 gold, 3 silver, 2 bronze and 6 other days for the tethersonde operations during SGP97. Tethersonde flights began around 7:00 a.m. local daylight time (1200 GMT) and continued hourly throughout the morning and every 1.5 hours in the afternoon until 5:00 p.m. local daylight time (2200 GMT). Each flight consisted of an ascent and descent, with thermodynamic and wind measurements every 10 seconds, with a maximum line length of 1000 m and an approximate vertical resolution of 2-5 m.

b. Other Data

In addition to the tethersonde system, radiosondes were released throughout the experiment every three hours by ARM at its Central Facility as well as at four Boundary Facilities (Figures 1 and 2, Table 3). The ARM soundings have a 2 second sampling interval for

thermodynamic quantities and a 10 second interval for winds. The Boundary Facilities are significant because they allow a direct estimation of the advection terms in (1) and (2).

Additional data collected at the Central Facility included surface fluxes from up to three eddy correlation systems as well as one Bowen ratio system. In this work, we focus on two of these systems: the University of Arizona (UA) eddy correlation system, which was available from Day 182 to 198; and the ARM/CART eddy correlation system, which was available throughout the experiment. As will be discussed, the ARM/CART system measured systematically higher sensible heat and lower latent heat fluxes throughout the experiment. Some of this can be explained by the different methods used to adjust the measured fluxes towards closure (Twine, personal communication, 1998; Houser, personal communication, 1998). However, this station-to-station variability (around 100 Wm^{-2} at midday, even though both were less than 5 m apart!), and can lead to significantly different results for direct estimates of the entrainment parameter, as will be discussed. On July 5 (Day 186), both the Twin Otter and Long-EZ flux aircraft sampled surface layer fluxes at the site, although unfortunately the flights were timed such that the inversion base was well above the maximum measurement height of the tethersonde; therefore these data have not been used directly in this study. The aircraft flux data and issues related to comparisons with surface towers are discussed in MacPherson et al. (1999), and much of their discussion is relevant here. Details on all SGP97 datasets, including QA/QC procedures as well as a description of the experiment itself are available via the SGP97 data archive site (http://daac.gsfc.nasa.gov/CAMPAIGN_DOCS/SGP97/sgp97.html).

4. Regional Flux Estimation

Given a tethersonde ascent-descent pair, we may solve (3) for $F_{s\theta} = \overline{\rho w' \theta'}_s$ using either assumption (4) or (5) and given an estimate of the advective term. In this work, we consider three basic advection estimates: (i) A "direct" method from analysis of surrounding radiosonde data; (ii) Swiatek's (1992) method given by Equation (7); and (iii). no advection. The height of the inversion base is estimated using a combination of automated and manual techniques, with the values given in Table 4. As an *a priori* test of the method, we first chose a standard value of A_R =0.2 and computed fluxes for each ascent-descent pair listed in Table 4 using all three advection estimates described above. We then compared this with the observed surface fluxes computed by averaging that measured by the two ECOR stations. Scatterplots illustrating the results are shown in Figures 3, 4, and 5, and RMS Errors and Bias summary statistics for the SGP97 campaign are given in corresponding Tables 5, 6 and 7. Figures 3 and 4 illustrate independent solutions for the sensible and latent heat fluxes obtained by solving the conservation of heat and moisture equations, respectively. The large scatter and bias in Figure 4 (RMS approx. 330 Wm^{-2}; Bias approx. –150 Wm^{-2}) as compared to Figure 3 (RMS approx. 54 Wm^{-2}; Bias approx. -20 Wm^{-2}) indicates that for this dataset, it is preferable to solve for sensible heat flux directly and solve for latent heat flux as a residual. Figure 5 illustrates the same results when the values in Figure 3 for sensible heat flux are used along with the average available energy (Rn-G) in (10) to estimate latent heat as a residual (RMS approx. 54; Bias approx. 15). These results are consistent with those of Kustas et al. (1994) and Lhomme et al. (1997). Lhomme et al. suggest that direct estimates of sensible heat are superior because the mixed layer is generally more well mixed in θ than in q, as evidenced by nearly vertical profiles of θ.

As Table 4 illustrates, all tethersonde profiles containing the inversion were launched before 1600 GMT (1100 LDT). Therefore, it would seem that during the morning transition, when significant ABL growth occurs due to entrainment of the overlying residual layer, a higher A_R value may be expected. In fact, before the ARM/CART ECOR data was available, the authors estimated a significantly higher value of A_R based on only the UA ECOR data. To better illustrate the difficulties in using a single source of data to evaluate uncertainties in the conservation approach, Figures 6 and 7 show the sensible and latent heat flux estimates for Day 186 (July 5, 1997). Reasonable (i.e. within the station standard error of 65 Wm^{-2}) agreement between the conservation estimates and the surface eddy corrrelation stations is indicated. Also shown on this day are the fluxes measured by two aircraft (the Long-EZ and the Twin Otter), and although these fluxes were not available during the times when the tethersonde was above the inversion, they illustrate the difficulty estimating "regional" flux parameters from surface towers.

5. Advection

Although the tethersonde was restricted to light to moderate wind conditions, an attempt was made to assess the effect of advection. Three representations were considered: (i) Direct estimation from surrounding radiosondes, as described below (ii) Swiatek's (1992) estimate of advection (7); and (iii) no advection. In order to calculate a direct advection estimate, we may utilize the three-hourly soundings at the Central and Boundary facilities (Figure 1, Table 2). To compute this estimate, first the winds and thermodynamic quantities from the soundings are analyzed (i.e. interpolated) onto a regular grid with spacing 5 km in the horizontal and 50 meters in the vertical. The horizontal grid is used to compute spatial gradients $\frac{\Delta\theta_n}{\Delta x_n}$ along the wind

directions u_n at each vertical level n. Given the spatial gradients, the vertically integrated advection term is calculated as follows:

$$\int_0^{Z_i} u \frac{\partial \theta}{\partial x} dz = \sum_{n=1}^{N} u_n \frac{\Delta \theta_n}{\Delta x_n} \Delta z_n \tag{11}$$

where N is the number of vertical levels up to Z_i, n is the vertical level index and, Δx_n is aligned with the wind direction. Variants of the direct approach included exchanging the tethersonde and the radiosonde at the as the source of data at the central facility. In general, the results from both variants were quite similar.

As shown in Figures 3, 4 and 5 and Tables 5, 6, and 7, the various advection approaches had little effect on the accuracy of flux estimates. This behavior is consistent with that found by Lhomme et al. (1997) and is reasonable given that the tethersonde could only fly in light to moderate winds.

Figure 8 compares the Swiatek estimate of advection from (7) with the direct estimates. While there is considerable scatter, the results suggest that there is no systematic bias in the Swiatek method as compared to the direct estimates.

5. The Diurnal Cycle of Heat Entrainment

Given estimates of the storage (or tendency) term as well as the advection term and surface sensible heat flux, one may directly calculate the inversion level flux following (3) and thereby estimate the entrainment parameter A_R, following (5). Derived entrainment parameter summary statistics are given in Table 8, where the mean value is 0.33 ± 0.32. We examined the behavior of A_R with parameters in the Tennekes (1973) model including $\overline{w'\theta'}_s$, u_*, T, and Z_i as well as other parameters. We found no significant relationships between A_R and other variables,

except for the slight suggestion of a relationship similar to that noted by Kustas and Brutsaert (1987b), where as shown in Figure 9, there is considerable scatter but some suggestion of a trend of decreasing A_R with increasing H.

Related to the trend in H is the diurnal cycle of convective boundary layer development driven not only by surface heating (via buoyant production) but also by the structure of the free atmosphere and the dynamics of shear production of turbulent kinetic energy (TKE) near the entrainment zone. Because our data focused on local times from 0700 to 1200, we noted a significant variability in A_R, which seemed to decrease with time. By combining our data with those of Kustas and Brutsaert (1987b) and plotting them versus local time in Figure 10, one recognizes what appears to be a significant diurnal cycle in the variance of A_R. We hypothesize that this diurnal cycle could be obtained by higher order parameterizations of A_R both in terms of the entrainment dynamics (e.g. TKE production, as in Tennekes (1973) and Dreidonks (1982)) and surface to inversion mixing, perhaps as a function of the surface and inversion Bowen ratios as in Betts (1992). One other estimate of A_R is shown on Figure 10—that derived from the application of (6) with a=0.2, b=5 and mean kinematic heat flux and shear velocity from the eddy correlation stations. These data suggest that if some of the variance in A_R could be explained, the accuracy and applicability of this simple mixed layer budget method could be extended for use under many conditions, including the morning transition period considered here.

6. Conclusions

We have demonstrated that the ABL conservation approach applied to hourly tethersonde data from the SGP97 field experiment, even with the "standard" entrainment parameter value A_R =0.2, yields good estimates of sensible heat flux with relatively simple representations of advection and entrainment. Application of the same method for direct estimation of latent heat flux performs quite poorly compared to estimation of latent heat flux as a residual using the sensible heat flux combined with the available energy from surface stations.

Three advection estimation techniques were examined and had only minor effects on the derived sensible heat flux estimates. In particular, Swiatek's (1992) approach seems to perform quite well, although we cannot extend this conclusion to windy regimes since our tethersonde deployment was limited to light to moderate wind conditions.

The entrainment parameter A_R was estimated directly using ABL conservation solutions and surface eddy correlation flux data. Following the arguments of Carson (1973) we find that there is considerable uncertainty associated with specification of A_R, and that its variance exhibits a pronounced diurnal cycle. While it is difficult to define a representative value, we find that an average value of A_R =0.3 $\pm$ 0.3 over the time period from 700 LT to 1200 LT yields flux estimates with an RMS error of about 55 Wm^{-2} and a bias of about 15 Wm^{-2}.

One limitation of our study is that a true estimate of regional sensible heat flux is unavailable. The eddy correlation system only represents a small region, with a fetch on the order of 100s of meters while the tethersonde can have a fetch on the order of 10-100 km.

Therefore, ideally a network of flux instruments or aircraft data could be used in order to gain a better measure of regional sensible heat flux for comparison with the tethersonde flux estimates. An area weighted flux from several flux stations (when available) would perhaps yield more appropriate values for comparisons with the tethersonde estimates, but the current analysis suggests that the RMS error is well within the between station variability we might expect.

The simplified conservation equations in this work retain terms representing only the advection and entrainment of heat and moisture. It is critical to examine the dynamics of other processes, including radiative and horizontal flux divergence in order to improve estimates of regional heat and moisture fluxes.

Acknowledgements

This work was funded through NASA/GSFC Contract NAG5-5146. This support is gratefully acknowledged. We express our appreciation to the following organizations and people for their support during SGP97: Mr. Les Showell of NOAA's National Severe Storms Laboratory (NSSL); and DOE's Atmospheric Radiation Measurement/Cloud and Radiation Testbed (ARM/CART) Central Facility. Surface flux data provided by Dr. Paul Houser, NASA/GSFC and Ms. Tracy Twine, University of Wisconsin.

References

Betts, A. K., 1973: A composite mesoscale cumulonimbus budget. *J. Atmos. Sci.*, **30**, 597-610.

Betts, A. K., 1992: FIFE atmospheric boundary layer budget methods. *J. Geophys. Res.*, **97**, 18,523-18,531.

Betts, A. K., R. L. Desjardins, J. I. MacPherson, and R. D. Kelly, 1990: Boundary-layer heat and moisture budgets from FIFE. *Bound.-Layer Meteor.*, **50**, 109-137.

Betts, A. K., R. L. Desjardins, and J. I. MacPherson, 1992: Budget analysis of the boundary layer grid flights during FIFE 1987. *J. Geophys. Res.*, **97**, 18,533-18,546.

Brutsaert, W., 1987: Nearly steady convection and the boundary layer budgets of water vapor and sensible heat. *Bound.-Layer Meteor.*, **39**, 283-300.

Brutsaert, W., and W. P. Kustas, 1987: Surface water vapor and momentum fluxes under unstable conditions from a rugged-complex area. *J. Atmos. Sci.*, **44**, 421-431.

Brutsaert, W., and M. B. Parlange, 1992: The unstable surface layer above forest: Regional evaporation and heat flux. *Water Resour. Res*, **28**, 3129-3134.

de Bruin, H. A. R., 1983: A model for the Priestly-Taylor α. *J. Clim. Appl. Meteor.*, **22**, 572-578.

Carson, D. J., 1973: The development of a dry inversion-capped convectively unstable boundary layer. *Quart. J. Roy. Meteor. Soc.*, **99**, 450-467.

Driedonks, A. G. M., 1982: Models and observations of the growth of the atmospheric boundary layer. *Bound.-Layer Meteor.*, **23**, 283-306.

Hipps, L.E., E. Swiatek, and W. P. Kustas, 1994: Interactions between regional surface fluxes and the atmospheric boundary layer over a heterogeneous watershed. *Water Resour. Res.*, **30**, 1387-1392.

Jackson, T., 1997: Southern Great Plains 1997 (SGP97) Hydrology Experiment Plan. URL http://hydrolab.arsusda.gov/sgp97/explan/.

Kustas, W. P., and W. Brutsaert, 1987a: Budgets of water vapor in the unstable boundary layer over rugged terrain. *J. Clim. Appl. Meteor.*, **26**, 607-620.

Kustas, W. P., and W. Brutsaert, 1987b: Virtual heat entrainment in the mixed layer over very rough terrain. *Bound.-Layer Meteor.*, **38**, 141-157.

Kustas, W. P., L. E. Hipps, and K. S. Humes, 1994: Calculation of basin-scale surface fluxes by combining remotely sensed data and atmospheric properties in a semiarid landscape. *Bound.-Layer Meteor.*, **73**, 105-123.

Lhomme, J.-P., B. Monteny, and P. Bessemoulin, 1997: Inferring regional surface fluxes from convective boundary layer characteristics in a Sahelian environment. *Water Resour. Res.*, **33**, 2563-2569.

MacPherson, J. I., R. Dobosy, S. Verma, W. P. Kustas, J. H. Prueger and A. Williams, 1999: Intercomparisons between flux aircraft and towers in SGP97. *Preprint volume: AMS 14th Conference on Hydrology, Dallas, Texas, 10-15 January 1999,* 125-128.

McNaughton, K. G., and T. W. Spriggs, 1986: A mixed-layer model for regional evaporation. *Bound.-Layer Meteor.*, **34**, 243-262.

Munley, W. G., and L. E. Hipps, 1991: Estimation of regional evaporation for a tallgrass prairie from measurements of properties of the atmospheric boundary layer. *Water Resour. Res.*, **27**, 225-230.

Stull, R. B., 1988: *An Introduction to Boundary Layer Meteorology*, Kluwer Academic Publishers, Dordrecht, 666 pp.

Sugita, M., and W. Brutsaert, 1990: Regional surface fluxes from remotely sensed skin temperature and lower boundary layer measurements. *Water Resour. Res*, **26**, 2937-2944.

Sugita, M., T. Hiyama and I. Kayane, 1997: How regional are the regional fluxes obtained from lower atmospheric boundary layer data?. *Water Resour. Res.*, **33**(6), 1437-1445.

Swiatek, E., 1992: *Estimating regional surface fluxes from measured properties of the atmospheric boundary layer in a semiarid ecosystem.* M. S. Thesis, Utah State University, Logan.

Tennekes, H., 1973: A model for the dynamics of the inversion above a convective boundary layer. *J. Atmos. Sci.*, **30**, 558-567.

Figures

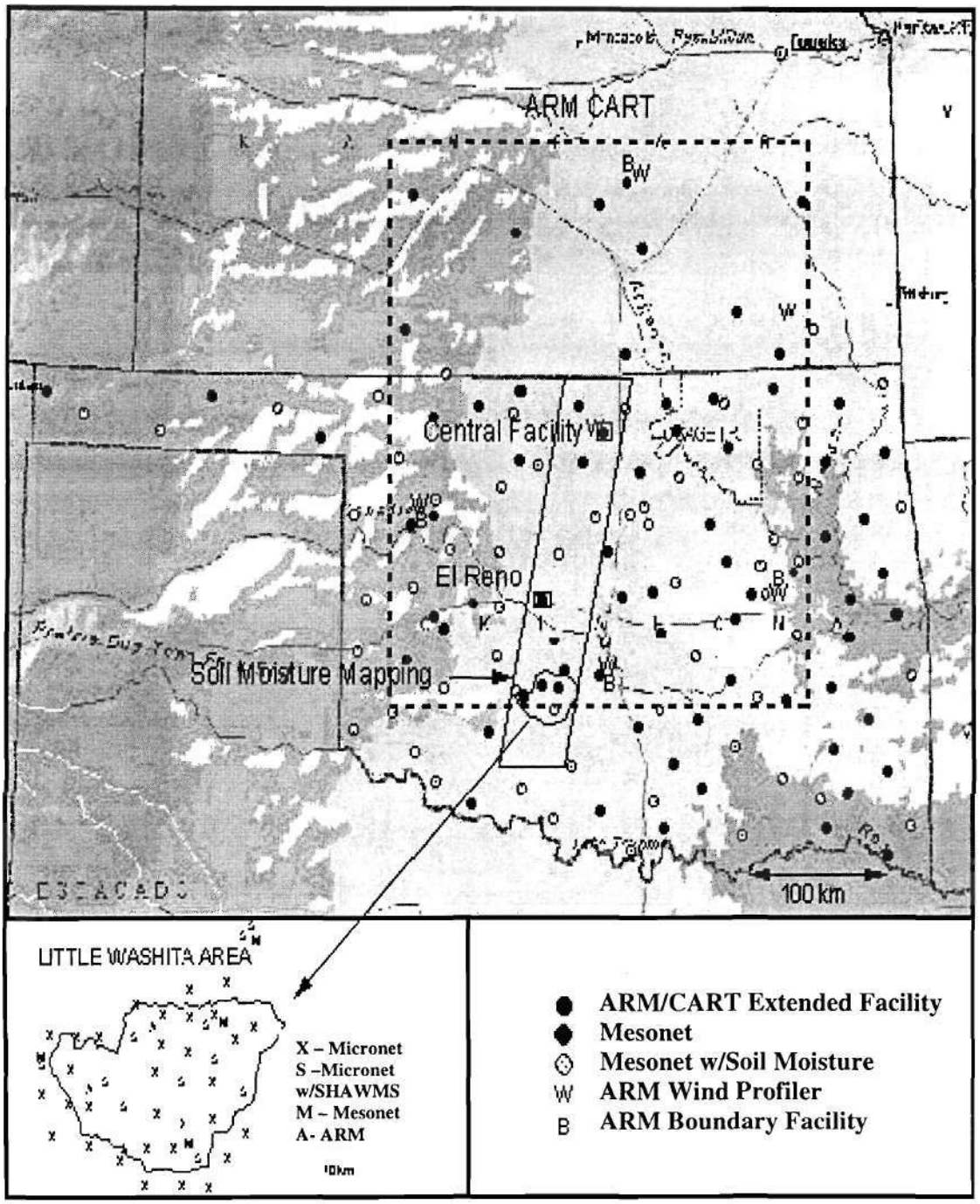

Figure 1. SGP '97 experimental domain showing locations of ARM/CART domain, ARM Central Facility and four ARM Boundary Facilities.

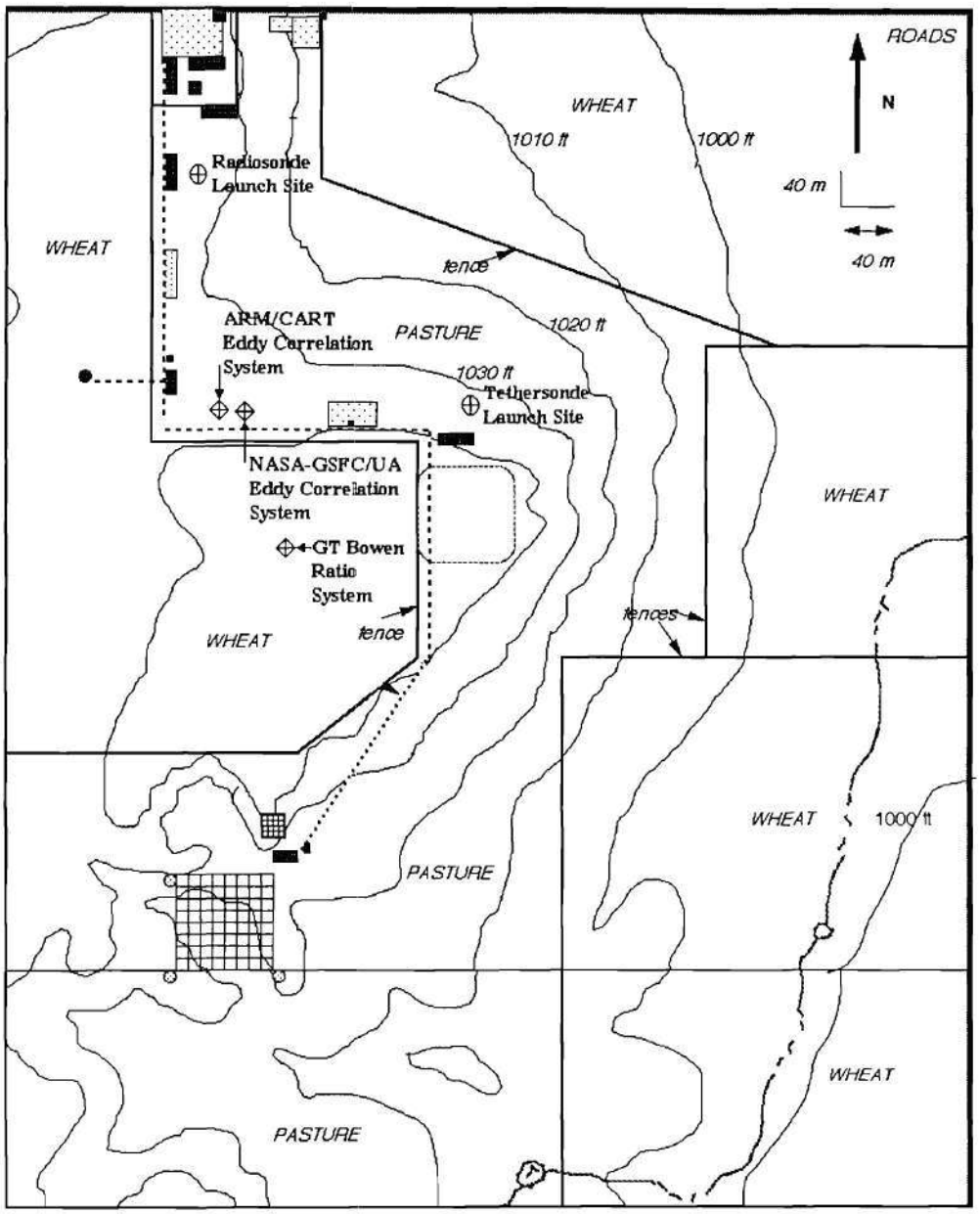

Figure 2. ARM Central Facility experimental domain showing locations of the radiosonde and tethersonde launch sites, eddy correlation systems, and the Bowen ratio system

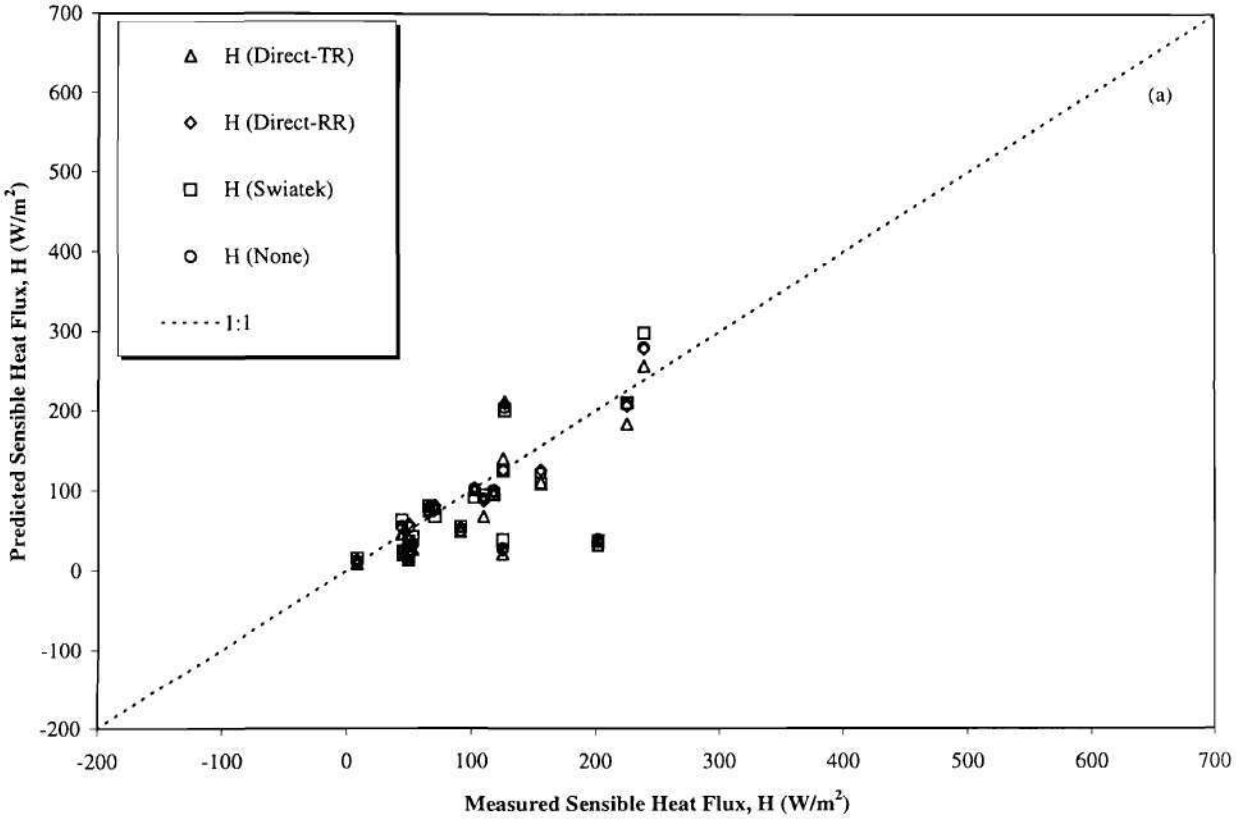

Figure 3. Sensible heat fluxes predicted via the ABL conservation approach versus average ECOR surface sensible heat fluxes for SGP97. Results shown use the *a priori* entrainment parameter estimate A_R=0.2 and symbols represent various advection estimation procedures.

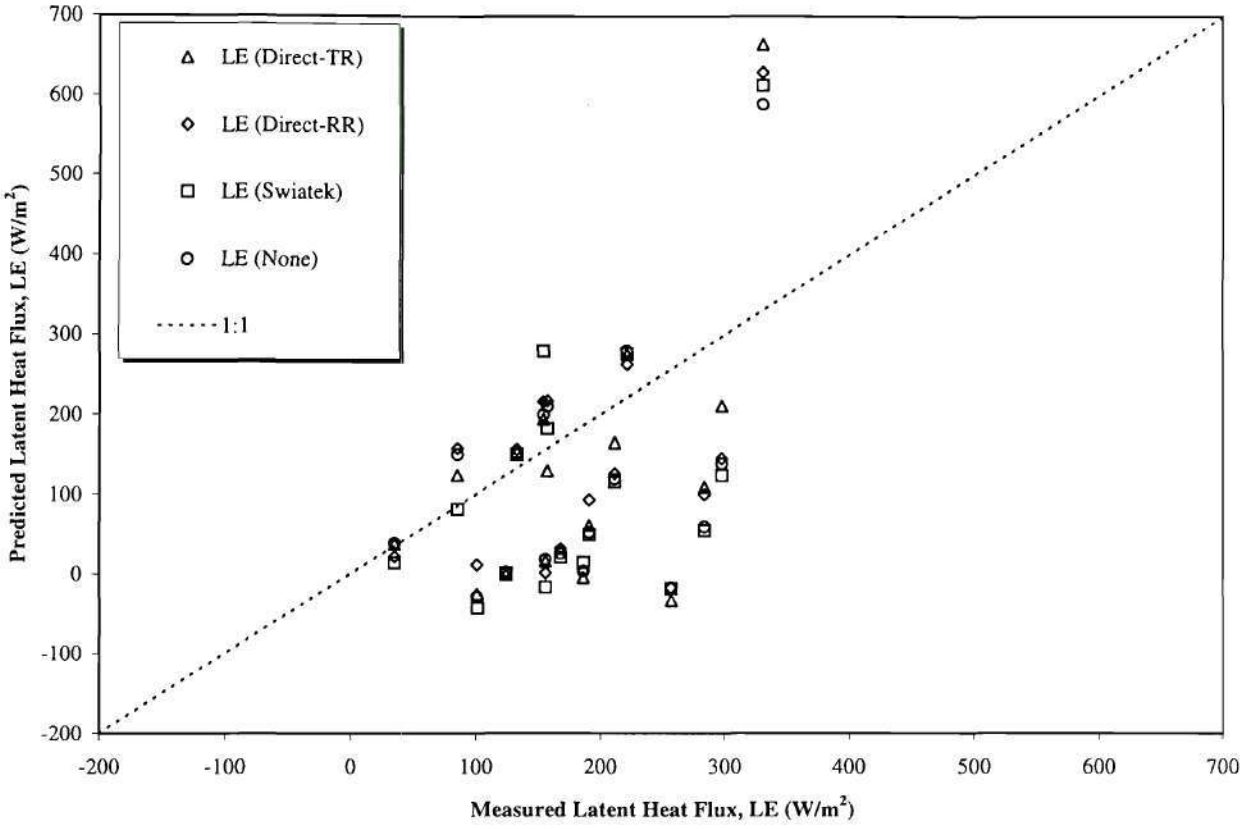

Figure 4. Same as Figure 3, but for Latent Heat Flux.

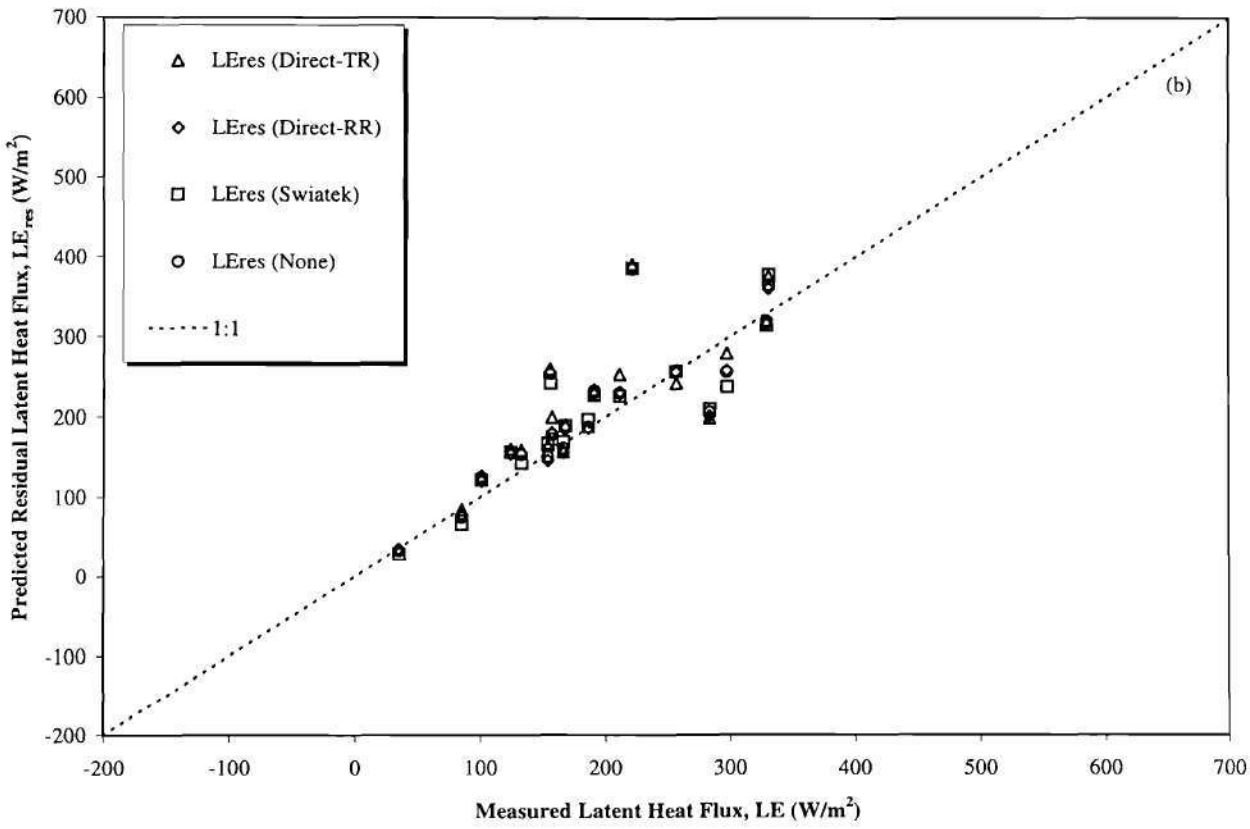

Figure 5. Same as Figure 3, but showing Latent Heat flux estimated as a residual using sensible heat estimates shown in Figure 3 and average available energy (Rn-G) measured at the ECOR stations.

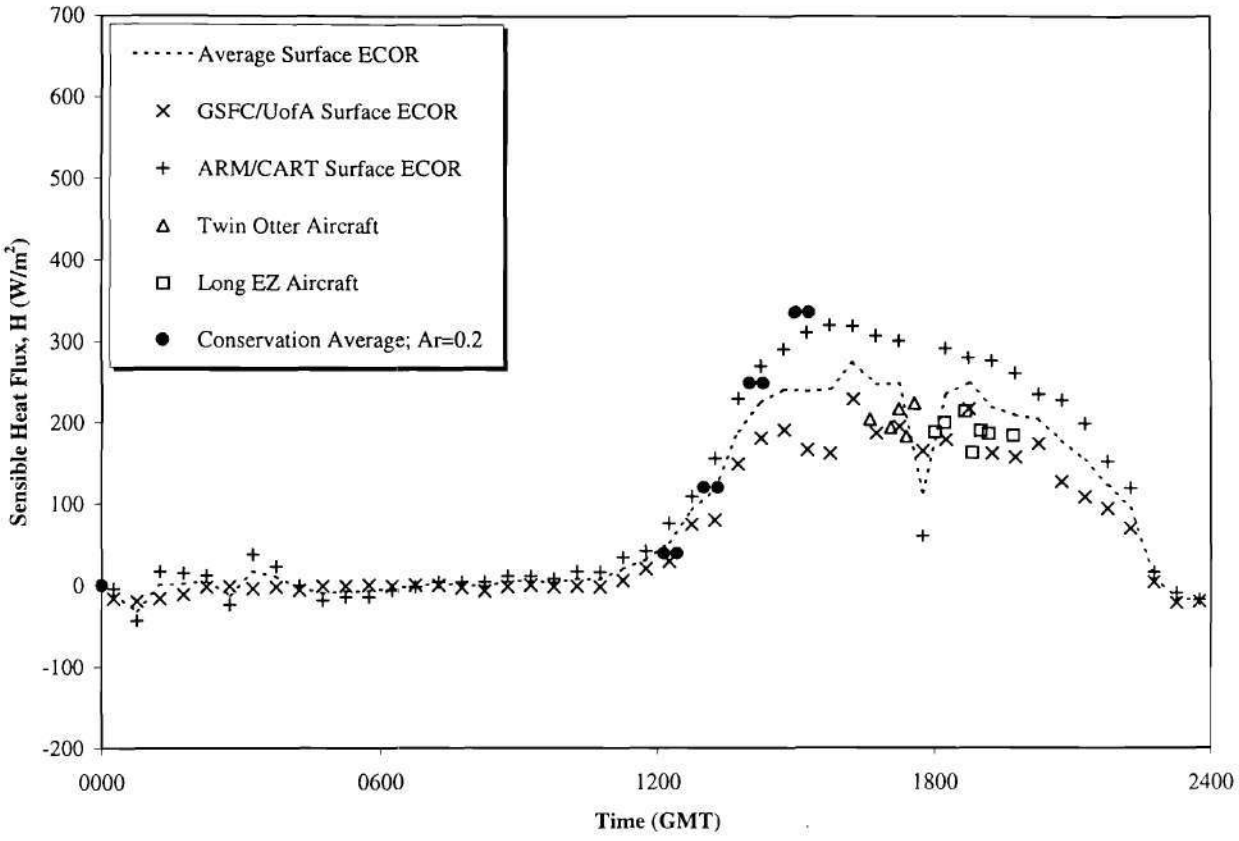

Figure 6. Sensible heat flux for DOY 186 (July 5, 1997) estimated via conservation approach using A_R=0.2. Solid circles represent the average among the various advection estimation methods, and data shown is from an Eddy Correlation (ECOR) flux stations and flux aircraft at the site. Note that no tethersonde flux estimates are possible after about 1600 GMT once Z_i exceeds the tether line length (1000m).

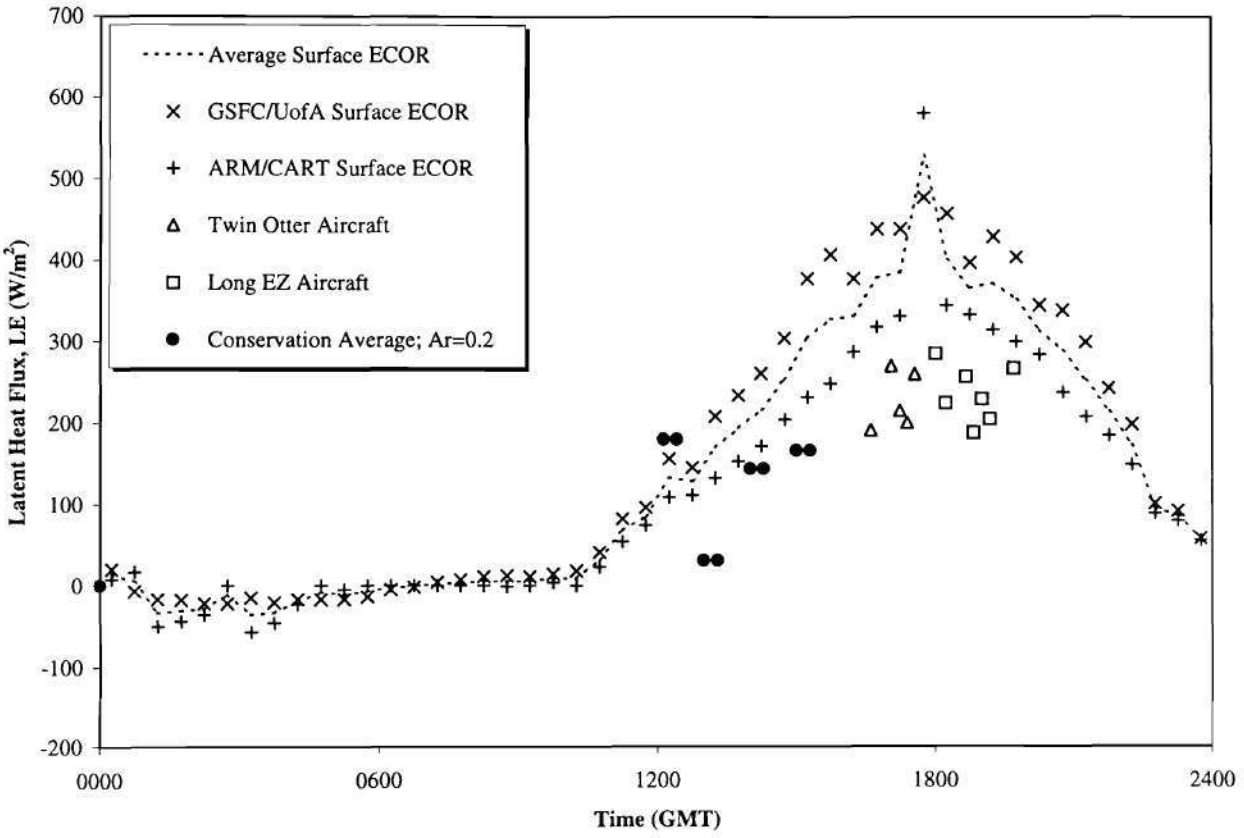

Figure 7. Similar to Figure 6, except showing Latent Heat flux estimated as a residual using sensible heat estimates shown in Figure 6 and average available energy (Rn-G) measured at the ECOR stations.

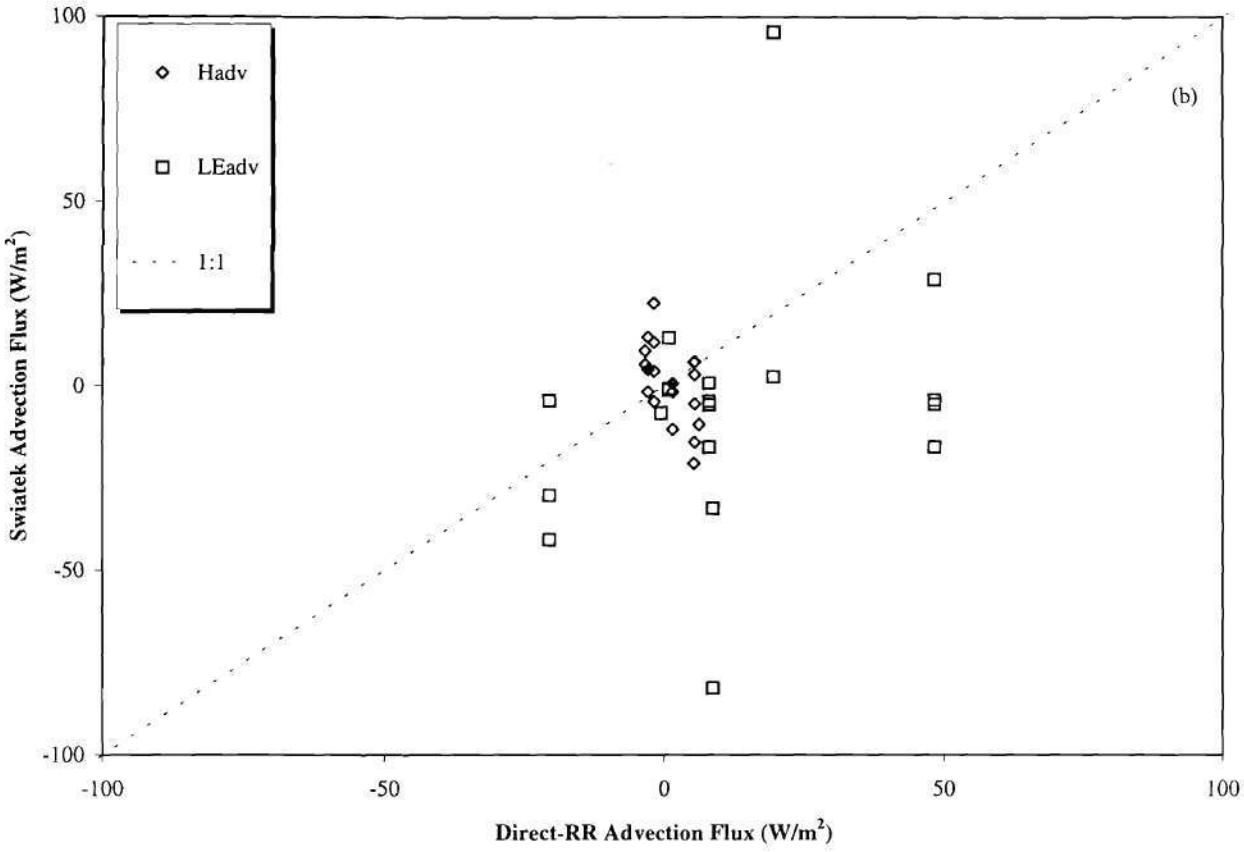

Figure 8. Swiatek's (1992) advection estimate versus direct advection estimate computed using ARM/CART boundary facility data as well as tethersonde data analyzed to a regular grid.

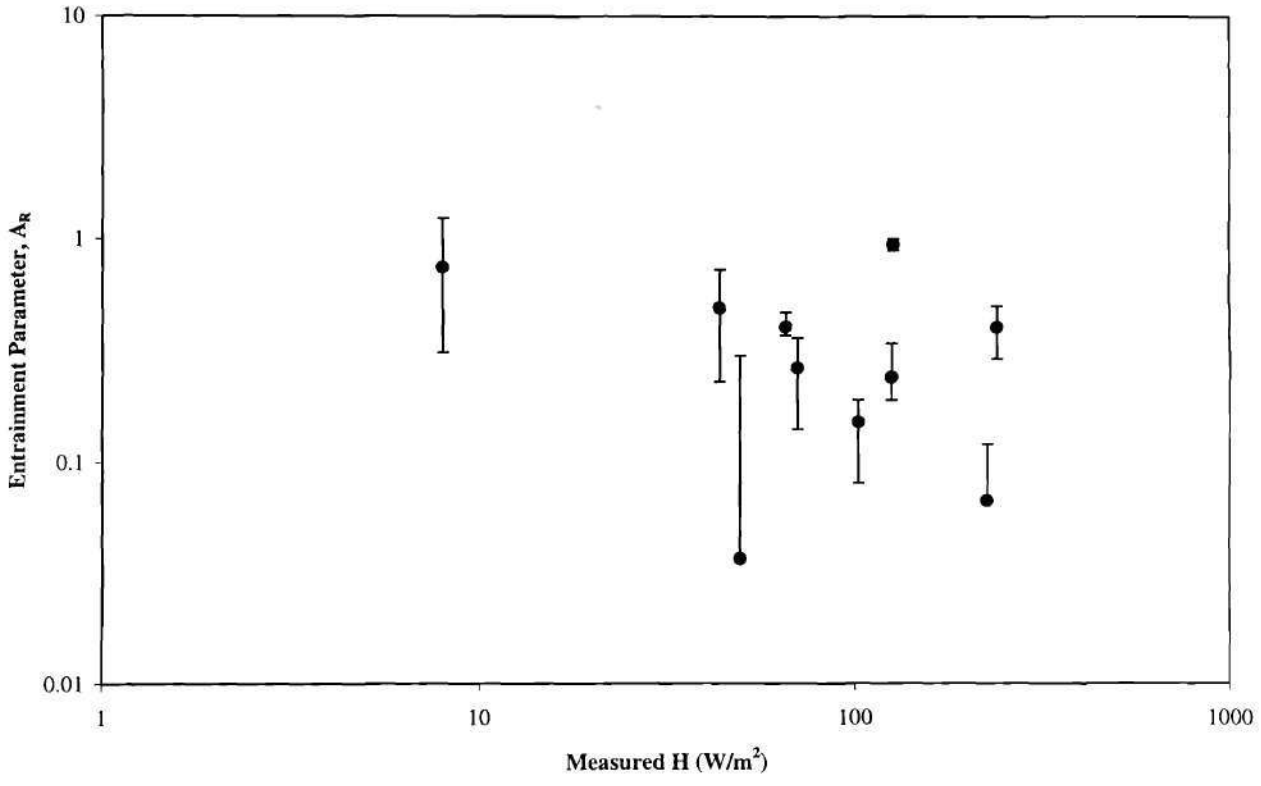

Figure 9. Derived entrainment parameter versus surface sensible heat flux, where there is a suggestion of decreasing values with increasing H. Errorbars represent variability in A_R estimates among the three advection approaches.

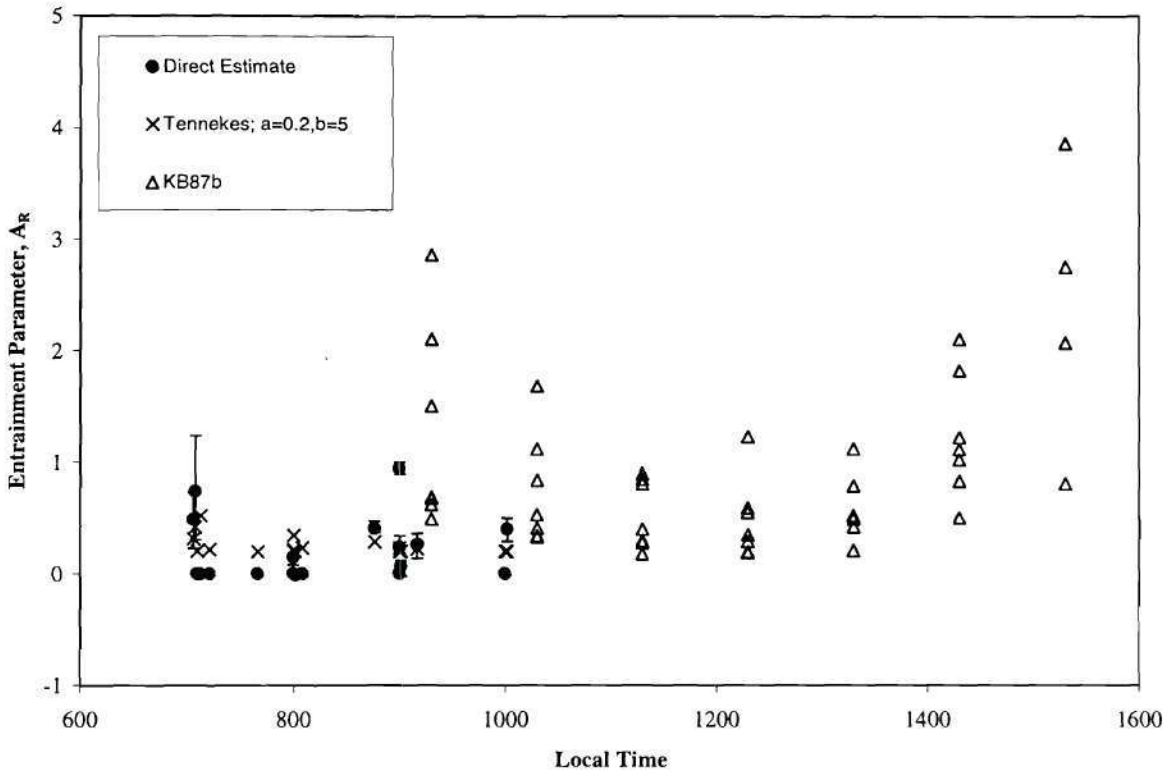

Figure 10. Diurnal cycle of the entrainment parameter A_R. Shown are direct estimates with errorbars representing variability among the three advection approaches, as well as direct estimates from the Tennekes model (6). KB87b represents the values shown in Kustas and Brutsaert (1987b).

Tables

Table 1. Tethersonde flights during SGP97 with maximum altitude and corresponding pressure achieved that day as well as assigned ranking

Date	DOY	Number of Flights	Maximum Altitude (m AGL)	Pressure at Maximum Altitude (mb)	Ranking
6/18/97	169	5	600	908.8	Silver
6/19/97	170	2	121	959.3	Other
6/22/97	173	3	619	909.3	Bronze
6/25/97	176	7	738	895.4	Gold
6/26/97	177	2	486	925.7	Other
6/27/97	178	7	700	901.3	Silver
6/28/97	179	1	212	948.4	Other
6/29/97	180	1	200	950.2	Other
7/2/97	183	2	658	901.0	Other
7/3/97	184	8	566	910.5	Silver
7/4/97	185	5	675	904.4	Bronze
7/5/97	186	9	778	893.4	Gold
7/6/97	187	8	993	869.6	Gold
7/14/97	195	6	790	890.6	Gold
7/15/97	196	1	330	940.7	Other
7/16/97	197	8	697	900.6	Gold

Table 2. Tethersonde flight rankings and corresponding criteria.

Rank	Criteria
Gold	>7 flights/day Calm to light winds Altitude > 700 m AGL
Silver	5-6 flights/day Light to moderate winds Altitude 500-700 m AGL
Bronze	3-4 flights/day Moderate to high winds Altitude < 500 m AGL
Other	< 3 flights/day High winds Miscellaneous problems/weather conditions

Table 3. ARM radiosonde and tethersonde launch locations. BF indicates Boundary Facility and CF indicates Central Facility.

Site Name	Location	Elevation (m MSL)	Latitude (Decimal Degrees)	Longitude (Decimal Degrees)
BF1	Hillsboro, KS	447	38.305 N	97.301 W
BF4	Vici, OK	622	36.071 N	99.204 W
BF5	Morris, OK	217	35.688 N	95.856 W
BF6	Purcell, OK	344	34.969 N	97.415 W
CF1	Lamont, OK	313	36.609 N	97.487 W
Tethersonde	Lamont, OK	313	36.606 N	97.485 W

Table 4. Tethersonde flight dates (DOY in 1997), times (GMT), inversion base elevation (Zi) and pressure (Pi), and mean wind speed (WS) and direction (WD). "a" and "d" indicate ascent or descent.

DOY	GMT	a (ascent) / d (descent)	Z_i (m MSL)	P_i (mb)	WS (m/s)	WD (degrees)
173	1207	a	342	972	2.1	45
173	1235	d	360	970	2.1	45
176	1238	a	355	970	0.0	50
176	1247	d	364	969	0.0	50
176	1320	a	454	959	5.4	186
176	1341	d	435	961	5.4	186
176	1408	a	537	951	6.4	220
176	1436	d	577	946	6.4	220
178	1205	a	608	942	3.1	145
178	1231	d	356	970	3.1	145
178	1300	a	459	960	5.9	207
178	1336	d	458	960	5.9	207
178	1401	a	590	946	5.3	179
178	1428	d	636	941	5.3	179
183	1240	a	365	967	2.0	264
183	1321	d	611	940	2.0	264
183	1346	a	528	949	9.6	33

183	1425	d	531	948	9.6	33
184	1204	a	361	966	5.0	140
184	1237	d	376	965	5.0	140
184	1305	a	464	956	6.1	177
184	1333	d	557	946	6.1	177
185	1410	a	585	949	4.1	277
185	1428	d	697	936	4.1	277
186	1213	a	346	977	3.5	159
186	1242	d	396	970	3.5	159
186	1301	a	440	966	3.2	143
186	1331	d	531	955	3.2	143
186	1401	a	622	946	5.2	160
186	1430	d	857	919	5.2	160
186	1501	a	952	909	5.5	166
186	1530	d	991	904	5.5	166

Table 4 (cont.). Tethersonde flight dates (DOY in 1997), times (GMT), inversion base elevation (Zi) and pressure (Pi), and mean wind speed (WS) and direction (WD). "a" and "d" indicate ascent or descent.

DOY	GMT	a (ascent) / d (descent)	Z_i (m MSL)	P_i (mb)	u_m (m/s)	u_{dir} (degrees)
187	1205	a	344	973	2.3	140
187	1234	d	322	976	2.3	140
187	1300	a	428	965	2.9	164
187	1329	d	430	964	2.9	164
187	1400	a	523	955	4.1	191
187	1429	d	618	944	4.1	191
195	1206	a	429	962	1.7	109
195	1235	d	432	961	1.7	109
195	1300	a	423	963	1.7	110
195	1327	d	509	954	1.7	110
195	1400	a	684	935	2.7	66
195	1428	d	652	939	2.7	66
195	1500	a	669	937	2.9	108
195	1525	d	711	933	2.9	108
197	1208	a	345	973	5.4	158
197	1227	d	354	972	5.4	158

197	1300	a	375	970	7.1	180
197	1328	d	376	969	7.1	180
197	1400	a	394	969	8.4	186
197	1424	d	594	946	8.4	186

Table 5. Sensible heat flux RMS error and Bias (calculated-observed) using various advection estimate methods and values of the entrainment parameter. RR indicates radiosonde only and RT indicates radiosonde plus tethersonde. Swiatek's advection estimate is given by Equation (7).

Advection Estimate	A	RMS (W/m^2)	Bias (W/m^2)
Direct-RR	0.2	52	-15
Direct-RR	0.4	54	-28
Direct-RR	0.6	58	-38
Direct-RR	0.8	63	-45
Direct-RR	1	67	-51
Direct-TR	0.2	56	-27
Direct-TR	0.4	58	-38
Direct-TR	0.6	62	-46
Direct-TR	0.8	67	-53
Direct-TR	1	71	-58
Swiatek	0.2	52	-18
Swiatek	0.4	53	-30
Swiatek	0.6	57	-40
Swiatek	0.8	62	-47
Swiatek	1	67	-53
None	0.2	51	-19

None	0.4	53	-32
None	0.6	58	-41
None	0.8	63	-48
None	1	67	-54

Table 6. Same as Table 5, but for directly estimated latent heat flux.

Advection Estimate	A	RMS (W/m^2)	Bias (W/m^2)
Direct-RR	0.2	321	-150
Direct-RR	0.4	291	-156
Direct-RR	0.6	270	-160
Direct-RR	0.8	256	-163
Direct-RR	1	245	-166
Direct-TR	0.2	346	-158
Direct-TR	0.4	312	-162
Direct-TR	0.6	288	-166
Direct-TR	0.8	271	-168
Direct-TR	1	258	-170
Swiatek	0.2	328	-161
Swiatek	0.4	298	-165
Swiatek	0.6	277	-168
Swiatek	0.8	262	-171
Swiatek	1	251	-172
None	0.2	325	-154
None	0.4	295	-159
None	0.6	275	-163
None	0.8	260	-166

None	1	249	-168

Table 7. Same as Table 5, but for latent heat flux estimated as a residual using direct estimate of sensible heat flux and average available energy (Rn-G) from surface flux stations.

Advection Estimate	A	RMS (W/m^2)	Bias (W/m^2)
Direct-RR	0.2	52	16
Direct-RR	0.4	54	29
Direct-RR	0.6	58	38
Direct-RR	0.8	63	46
Direct-RR	1	67	52
Direct-TR	0.2	56	23
Direct-TR	0.4	58	35
Direct-TR	0.6	62	43
Direct-TR	0.8	67	50
Direct-TR	1	71	56
Swiatek	0.2	52	16
Swiatek	0.4	53	29
Swiatek	0.6	57	38
Swiatek	0.8	62	46
Swiatek	1	67	52
None	0.2	51	17

None	0.4	53	29
None	0.6	58	39
None	0.8	63	46
None	1	67	52

Table 8. Entrainment parameter values calculated using various advection estimation techniques. R+T indicates radiosonde plus tethersonde, and R only indicates radiosonde only. Swiatek's advection estimate is given as Equation (7).

Advection Method	Mean A_R	Standard Deviation
Direct (RT)	0.30	0.28
Swiatek	0.36	0.41
None	0.33	0.28
All Methods	**0.33**	**0.32**